

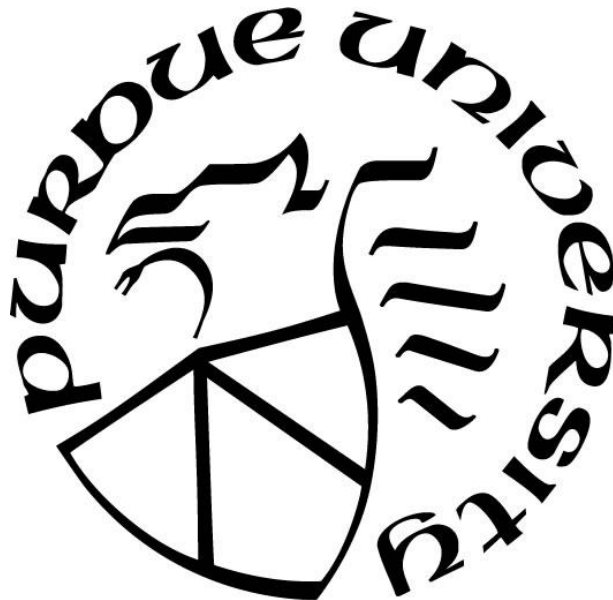
**BASO₄ NANOCOMPOSITE COLORED COOLING PAINT
AND
BIO-INSPIRED COOLING METHOD**

by
Peiyan Yao

A Thesis

*Submitted to the Faculty of Purdue University
In Partial Fulfillment of the Requirements for the degree of*

Master of Science in Mechanical Engineering



School of Mechanical Engineering

West Lafayette, Indiana

August 2020

**THE PURDUE UNIVERSITY GRADUATE SCHOOL
STATEMENT OF COMMITTEE APPROVAL**

Dr. Xiulin Ruan, Chair

School of Mechanical Engineering

Dr. Jong Hyun Choi

School of Mechanical Engineering

Dr. Amy Marconnet

School of Mechanical Engineering

Approved by:

Dr. Nicole L. Key

ACKNOWLEDGMENTS

First of all, I would like to express my sincere gratitude to Dr. Xiulin Ruan who offered me the opportunity to work on my current thesis. He has always shown great passion in the radiative heat transfer which undoubtedly encourages me to dedicate myself in this field. Being a talented researcher as well as an extremely patient mentor, Dr. Xiulin Ruan was always able to provide insightful suggestions and guidance in the past two years. It has absolutely been an honor for me to be in his group.

I would also like to show my deepest appreciation to committee members, Dr. Jong Hyun Choi and Dr. Amy Marconnet, for their support. In the past two years, I was also extremely lucky to have received tremendous mentoring and help from group members especially Dr. Xiangyu Li and Joseph Peoples. Dr. Xiangyu Li offered me the precious opportunity to join his research and learn the experiment methods in radiative cooling. Joseph Peoples as a senior and very talented PhD student also provided great help to me in the experiment.

Last but not the least, I want to thank to my parents who provided me the strongest support and confidence.

Thanks to everyone who was a part of my unforgettable experience at Purdue University. I hope my work in the colored radiative cooling paint as well as the bio-inspired cooling method can benefit our future research and contribute to the alleviation of global warming.

TABLE OF CONTENTS

LIST OF TABLES	5
LIST OF FIGURES	6
ABSTRACT	8
1. INTRODUCTION	9
2. COLORED RADIATIVE COOLING.....	14
2.1 Passive radiative cooling paint with TiO ₂ nanoparticles	14
2.2 Colored cooling paints with BaSO ₄ nanocomposite.....	16
2.3 Fabrication of colored cooling paints	17
2.4 Methodology of measurement	20
2.4.1 Introduction of Spectrometer.....	20
2.4.2 Outdoor experiment setup for colored cooling paint.....	21
2.5 Experimental results.....	22
2.5.1 Indoor Spectrometer test result.....	22
2.5.2 Outdoor test results of colored paint temperature.....	31
2.6 Further work in optimizing solar reflectance.....	40
2.6.1 Analysis tool	41
2.6.2 Modified Mie theory.....	41
2.6.3 Monte Carlo method.....	43
3. BIO-INSPIRED RADIATIVE COOLING	44
3.1 Desert snail.....	44
3.2 Seashell	45
3.3 Spectrometer test result.....	46
4. CONCLUSION AND FUTURE WORK	51
APPENDIX A. SEM PICTURES.....	53
REFERENCES	56

LIST OF TABLES

Table 1. Color paints materials	20
Table 2. Light Green paints comparison.....	30
Table 3. Yellow paints comparison	30
Table 4. Green paints comparison	31
Table 5. Blue paints comparison.....	31

LIST OF FIGURES

Figure 1. a) Solar irradiation and distribution. b) Transmittance in the sky window	10
Figure 2. Comparison between experimental temperature difference vs theoretical temperature difference	15
Figure 3. Holders for TiO ₂ paints	15
Figure 4. TiO ₂ paint outdoor experiment, West Lafayette, IN.....	16
Figure 5. Electron Scale	17
Figure 6. a) Probe of Sonifier and the holder. b) Sonifier driving machine	19
Figure 7. Tool used in controlling thickness.....	20
Figure 8. a) Spectrometer Lambda1050. b) The back. c) Inside.....	21
Figure 9. Outdoor experiment setup	22
Figure 10. Spectral reflectance of the Light Green paints.	23
Figure 11. Light Green color paints plot of transmittance.....	24
Figure 12. Yellow color paints plot of reflectance	25
Figure 13. Yellow color paints plot of transmittance	26
Figure 14. Green color paints plot of reflectance	27
Figure 15. Green color paints plot of transmittance	28
Figure 16. Blue color paints plot of reflectance.....	29
Figure 17. Blue color paints plot of transmittance.....	29
Figure 18. Oct.23 rd Light Green color paints outdoor experiment, West Lafayette, IN.....	33
Figure 19. Oct.23 rd Yellow color paints outdoor experiment, West Lafayette, IN.....	34
Figure 20. Oct.23 rd Green color paints outdoor experiment, West Lafayette, IN.....	35
Figure 21. Oct.23 rd Blue color paints outdoor experiment, West Lafayette, IN.....	36
Figure 22. Oct.28 th Light Green color paints outdoor experiment, West Lafayette, IN	37
Figure 23. Oct.28 th Yellow color paints outdoor experiment, West Lafayette, IN.....	38
Figure 24. Oct.28 th Green color paints outdoor experiment, West Lafayette, IN.....	39
Figure 25 Oct.28 th Blue color paints outdoor experiment, West Lafayette, IN	40
Figure 26. Showcase of Desert snail shell in transferring heat [17]	44
Figure 27. SEM pictures of the surface of Sand Dollar	45

Figure 28. SEM pictures of Marine Mollusks cross section.....	46
Figure 29. Radiative properties of sand dollar.....	47
Figure 30. Thin white shell radiative properties.....	48
Figure 31. Thick white shell radiative properties.....	49
Figure 32. Second thick white shell sample radiative properties.....	50
Figure 33. SEM picture of sand dollar with 25k Magnification.....	53
Figure 34. SEM picture of inside Marine mollusks with 357 Magnification.....	53
Figure 35. SEM picture of inside Marine Mollusks with 2K magnification.....	54
Figure 36. SEM picture of inside Marine Mollusks with 10K magnification.....	54

ABSTRACT

Radiative cooling is an approach that utilizes the material reflectance in solar spectrum to reflect solar irradiation and emit the energy to deep space (2.7K) through the transparent portion in atmosphere (8-13 μ m). Therefore, radiative cooling is a passive cooling method that can generate a large reduction in energy consumption in the cooling sector. Scientists have been researching on the best solution for passive radiative cooling, including the utilization of multi-layer techniques with a metallic base layer. However, the current solutions are usually not cost effective and thus limited in the commercial applications. We initially started with the experiment on single-layer cooling paints embedded with TiO₂ nanoparticles, and we were able to achieve a partial daytime radiative cooling effect of $60\frac{W}{m^2}$. Built upon our lab's success of full-daytime sub-ambient cooling based on BaSO₄-acrylic paints, we experiment with colored cooling paints based on BaSO₄ nanoparticles instead of TiO₂ nanoparticles. Our results show much enhanced solar reflectance while matching the color, indicating the potential for colored cooling paints, although outdoor tests have not shown significant temperature drop compared to commercial colored paints yet. At the same time, we also explore creatures with shells in nature for possible solutions. Seashells are collected and the microstructures and radiative properties are characterized. The results provide insights into bio-inspired radiative cooling solutions.

1. INTRODUCTION

In the modern society, energy consumption has become a crucial problem, and various topics have been brought up by researchers. Radiative cooling shows significant promise among all these technologies as it is able to greatly reduce the energy consumption utilized in cooling and thereby alleviate the global warming. The core idea of radiative cooling is to utilize the existence of nearly transparent portion in the atmosphere, which is also known as “sky window” between the range of $8\mu\text{m}$ and $13\mu\text{m}$, to emit thermal energy to the deep space. Therefore, radiative cooling is also known as a passive cooling method since it requires no power consumption to realize the cooling effect. The viability of this method is confirmed by the Wien’s Displacement Law, which states that the peak thermal emission takes places at $\lambda_{max}T = 2898\mu\text{m}\cdot\text{K}$. Considering a body with the temperature of 300K , it reaches peak emission at the wavelength of $10\mu\text{m}$ which is in the range of sky window. With the progress in radiative cooling, both daytime and night-time cooling can be achieved while the daytime cooling power usually plays a larger role in most of the cases. However, the fact of larger demands in the daytime cooling will not reduce the importance of the nighttime cooling. In order to achieve 24-hour continuous passive radiative cooling, the material needs to have both high emissivity in the sky window and high reflectance in the solar spectrum, which are hard to be achieved at the same time. Therefore, the selection of the materials becomes essential in achieving high radiative cooling performance.

Figure 1(a) shows the solar irradiation in UV/Vis/NIR bands and Figure 1(b) shows the transmittance of the atmosphere which is between the wavelength of $8\mu\text{m}$ and $13\mu\text{m}$. Sub-ambient daytime radiative cooling may be achieved with the threshold of 85% solar reflectance, and each 1% increase in the reflectance will result in $10\frac{\text{W}}{\text{m}^2}$ cooling power increase [1]. Both reflectance in solar spectrum and the transmittance in sky window are essential properties of the cooling paint materials.

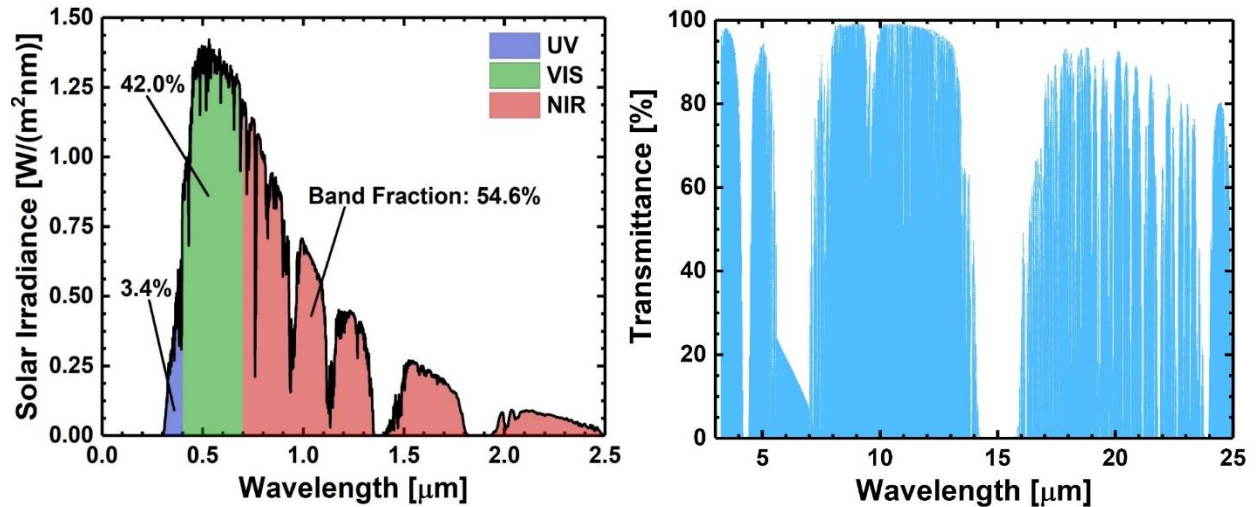


Figure 1. a) Solar irradiance and distribution. b) Transmittance in the sky window

Radiative cooling has been extensively studied in the literature. Nilsson et al. [2] demonstrated their works on studying ZnS pigmented polyethylene foils. According to their calculation, optimized ZnS pigmented foil should be able to show 0.82 of overall solar reflectance and 0.6 transmittance in the 8-13μm region. A cooling effect was predicted for 18 hours a day, with 3 hours in both morning and evening. They did not achieve the cooling effect under direct sunlight during the daytime but expected to decrease the heat load from solar irradiation by $43 \frac{W}{m^2}$.

Raman et al. [3] designed a radiative cooler device with seven alternating layers of hafnium dioxide (HfO₂) and silicon dioxide (SiO₂) on top of a composite layer of Ag-Ti, which are placed on the top of Si wafer. In this device, HfO₂ helps with the reflectance of solar irradiation and SiO₂ enhances the emittance in the sky window due to the exist of peak absorptivity near 9μm. The performance of this cooler is outstanding, providing $4.9 \text{ } ^\circ\text{C} \pm 0.15 \text{ } ^\circ\text{C}$ below the ambient air temperature under direct sunlight and a cooling power of $40.1 \frac{W}{m^2}$. However, the drawback is that the use of the nanostructured multilayer makes this device expensive. Furthermore, a nanoscale multilayer is not scalable in commercial use.

Huang and Ruan et al. [4] proposed a dual-layer coating with acrylic resin embedded with titanium dioxide(TiO₂) particles and carbon black particles. The TiO₂ particles embedded in the top layer is not absorptive in most of the solar spectrum, therefore it should be able to provide good solar

reflection. The carbon black has high absorptivity in the sky window and therefore can be utilized to emit heat in the sky window. In this design, both TiO₂ and carbon black are quite cost-effective compared to the materials used in Dr.Raman's work [3]. Also, both daytime and nighttime radiative cooling can be achieved using this design. The predicted daytime cooling power is $100\frac{W}{m^2}$ and nighttime cooling power is $180\frac{W}{m^2}$ when the surface is at the ambient temperature. According to the results, this dual-layer coating already shows great potential in radiative cooling. However, as the electron band gap of TiO₂ is around 3.2eV, this coating can still be quite absorptive in the ultra-violet range.

Kou et al. [5] also achieved passive radiative cooling under direct sunlight using the fused silica wafer coated with a polymer as top layer and a silver layer as the back reflector. Based on their results, this cooling device can reach 8.2°C below the ambient temperature with a cooling power of approximately $127\frac{W}{m^2}$. The cooling effect of their cooling device is excellent while the structure of their design is rigid.

Zhai et al. [6] demonstrated a metamaterial with high daytime and nighttime radiative cooling performance. The metamaterial consists of a visible transparent polymer encapsulating randomly distributed SiO₂ nanospheres, which is placed on a 200nm thick silver coating, which provide approximately 96% reflectance to solar irradiation. A cooling power of $93\frac{W}{m^2}$ under direct sunlight was achieved. All in all, the solutions mentioned previously mostly rely on a double-layer structure: metallic layer to provide the high solar reflectance and infrared emissive material layers to provide emittance to atmospheric transparent window. Common choices include SiO₂ [3], SiC [7], ZnS [2], TiO₂ [4], Ag [3, 5, 6] and so on. Some other innovative approaches can also be considered as good reference. These approaches take advantage of the porous structure to greatly increase the solar reflectance [8, 9, 10]. However, the thickness of coating in turn is increased, ranging from hundreds of micrometers to several millimeters. What is more, there is also design that blocks the solar irradiation on a narrow direction while allowing the emission of radiation in other direction to atmospheric transparent window [11].

Clearly, the existing solutions have one or more limitations such as high cost, low scalability, and the use of a metal layer which could hinder commercial applications. To address these limitations, it is a pertinent task to develop radiative cooling paints that are high performance, low cost, and compatible with commercial paint manufacturing technologies. In our initial design of experiment, single-layer nanoparticle-acrylic composites are fabricated to help achieve this goal. Nanoparticles are responsible for the solar reflectance [12], while either matrix or nanoparticles can provide high emittance in sky window. Therefore, the optimized radiative cooling performance requires the selected material to have a large bandgap to minimize the absorptivity of solar irradiation. At the same time, this material should not possess high reflectance in the sky window. If selected carefully, the nanoparticle size should be comparable to the solar spectrum wavelength and much smaller than the wavelength in the sky window. This way, the nanoparticles will not significantly scatter the photons in the sky window, while the strong scattering effect in the solar spectrum can lead to high reflectance to the solar irradiation. Under this circumstance, this composite should already have good performance in radiative cooling. Lastly, since acrylic is known to have high transparency in the visible range as well as strong emittance in sky window, nanoparticle-acrylic composite can therefore be fabricated by embedding the selected nanoparticles in the acrylic resin. However, the idea of single-layer radiative cooling device is challenging and requires a great amount of experiments to prove the potential in this design. According to recent studies, it is a more common approach of having a dual-layer or multi-layer device to achieve high solar reflectance or high emittance in the sky window.

We initially selected TiO_2 as the nanoparticle to be embedded in the acrylic to form a single-layer coating. TiO_2 has low absorptivity in most of the solar spectrum, which leads to considerably high reflectance to the solar irradiation. Moreover, because of the low cost and toxicity as well as the high refractive index, TiO_2 also has been very popular in commercial use. TiO_2 nanoparticles were optimized to have the particle size around 500nm according to our previous study [4]. In the outdoor experiment, the single-layer TiO_2 nanoparticle composites exhibited partial daytime cooling with the lower surface temperature than ambient temperature. It was able to achieve cooling power around $63 \frac{\text{W}}{\text{m}^2}$ during nighttime. Although the single-layer TiO_2 nanoparticle composite only showed partial daytime cooling, it was quite likely that the humidity after raining

negatively influenced the cooling effect [13]. Therefore, our TiO₂ nanocomposite still owns the potential of full daytime cooling in a drier environment.

We then considered BaSO₄ as it has been known for the high reflectance that could be comparable with Spectralon which is often used as reflectance standard [14]. Recent works from our lab have demonstrated full-daytime cooling with BaSO₄-acrylic paints. Hence, we use BaSO₄ instead of TiO₂ as the basis to develop color cooling paints. The colored paints show considerably higher reflectance in the solar spectrum than commercial paints while matching the color, implying the potential for cooler surface under the sun, although the outdoor test has not shown the expected performance yet.

Driven by the interests in approaches of achieving ultimate solar reflection, the interests of research were shared to several natural creatures that live in the most extreme environments. Silver ants and desert snails were the first targets studied due to their superior ability of surviving in the hottest places on the Earth. The key for silver ants to survive is the perfect internal reflection realized with the densely patterned triangular hair. The broadband high reflectance over NIR and visible range helps silver ants to maintain a safe body temperature under the direct sunlight in Saharan desert [15]. With the discovery from silver ants, desert snail drew our attention as well. Covered with CaCO₃ mainly shells, desert snails are able to survive in the desert even without water. As the surface temperature of the sand usually reaches 65°C, the shell surface can always be maintained at around 50°C. Similar to the desert snails, seashell was another type of creatures of interest as their shells are all mainly formed with CaCO₃. We conducted experiment on the seashells. Utilizing the techniques of analyzing their solar reflectance with spectrometer and observing the shell inner structures with SEM pictures, we were able to study the influencing factors to the solar reflectance hiding in these shells. Furthermore, these analysis results hopefully can be applied in the future research of radiative cooling method.

2. COLORED RADIATIVE COOLING

2.1 Passive radiative cooling paint with TiO₂ nanoparticles

One of the high-performance nanoparticles studied was the TiO₂ which has been a popular commercial white paint. We performed both indoor and outdoor experiments to test the paints embedded with TiO₂ nanoparticles. One of the critical models we used in expressing the radiative cooling system is shown as Equation 1,

$$h(T_s - T_{amb}) = h\Delta T = \alpha G - q''_{radiation}(T) - \frac{mC_p}{A} \frac{dT}{dt} \quad (1)$$

h accounts for the convective heat transfer coefficient with the ambient, T_s and T_{amb} represent the paint temperature and the ambient temperature respectively, α is account for the solar absorptance of the sample, G represents solar irradiation, $q''_{radiation}(T)$ shows the heat loss due to radiative effect, and $\frac{mC_p}{A} \frac{dT}{dt}$ is account for the heat capacity effect. As the paint is surrounded by the foam with extremely low thermal conductivity, the heat loss due to conduction could be neglected. Besides the conduction effect, heat capacity effect can also be neglected since the change of temperature per hour was small compared to other terms in the equation. With a feedback heater beneath the paint, the surface temperature can be heated to sync the ambient temperature. Therefore, when T_s is equal to T_{amb} , the radiative heat loss $q''_{radiation}$ is calculated by experimentally measured solar absorptance α multiplied by experimentally measured solar irradiation G plus the heater power. The convective heat transfer coefficient is assumed to be constant throughout the entire experiment time period. In the nighttime, solar irradiation $G=0$ and convective heat transfer coefficient h can be calibrated with $q''_{radiation}$. In the end, the temperature difference $(T_s - T_{amb})$ can be theoretically estimated based on the measured solar irradiation and absorptance. As can be observed in Figure 2, the theoretical estimation actually shows agreement with the experimental results.

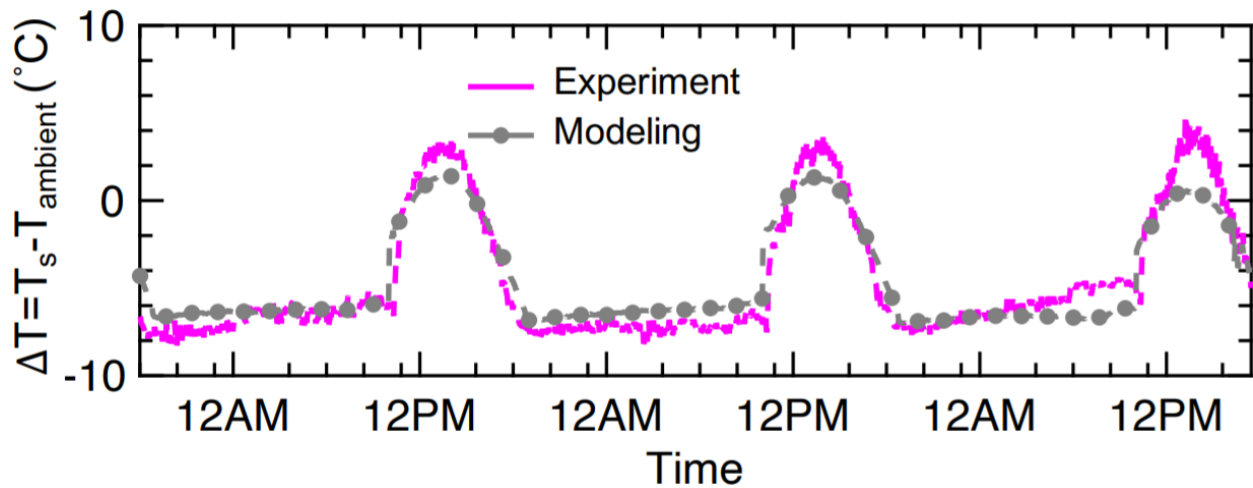


Figure 2. Comparison between experimental temperature difference vs theoretical temperature difference

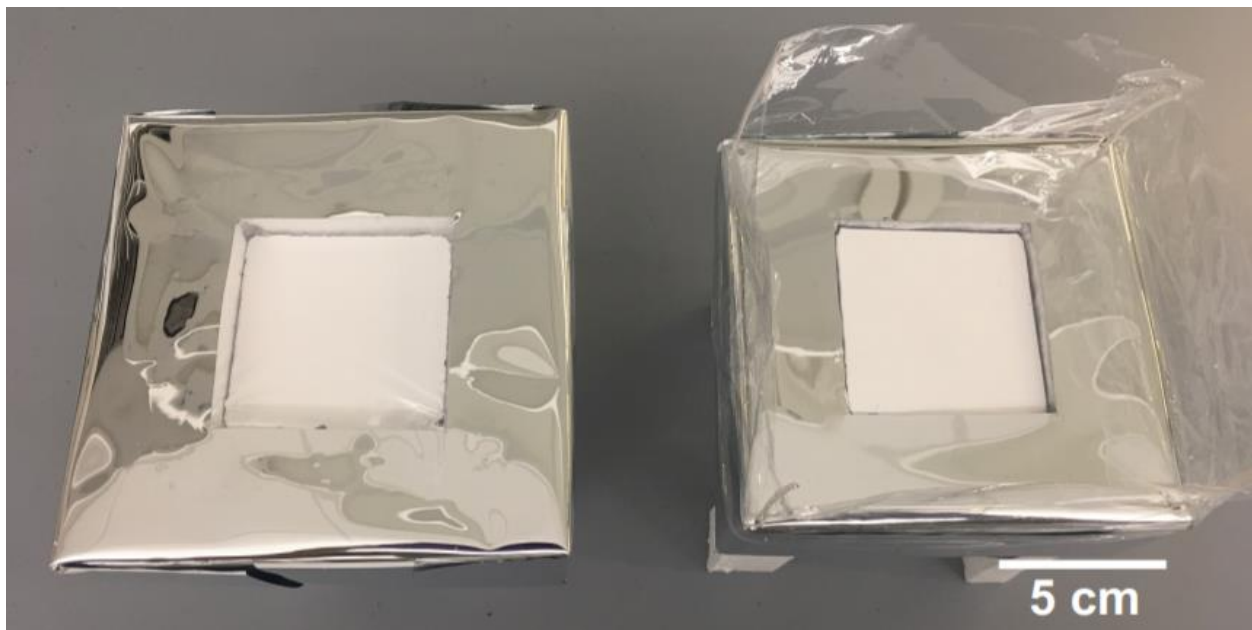


Figure 3. Holders for TiO₂ paints

The TiO₂ paints were fabricated by Xiangyu, former PhD student in our group, and the particle size was opted to be 500nm according to the previous study [4], which could provide a high reflectance in both visible and NIR range. The outdoor experiment setup was created as shown in Figure 3. Paint can be fitted in the middle of the holder and covered by the visibly transparent plastic film. And the temperature change during the experiment period was recorded by the thermal

couple and plotted with Matlab. The experiment was on Oct 16-19, 2017 in West Lafayette, IN and the experiment result is shown in Figure 4.

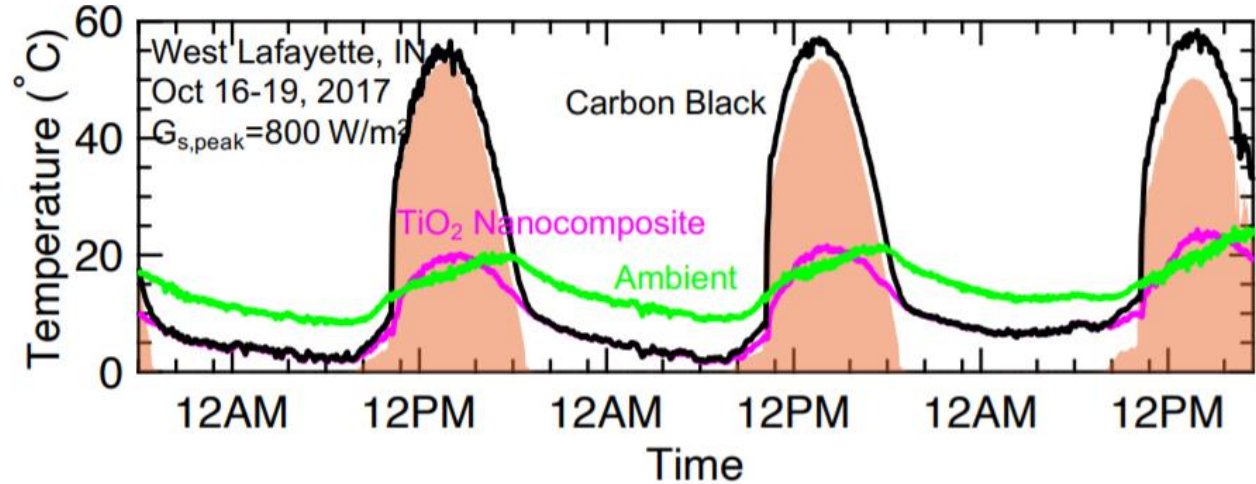


Figure 4. TiO₂ paint outdoor experiment, West Lafayette, IN

The shaded region represents the strength of solar irradiation and the temperature of Carbon Black sample is utilized as a comparison shown as black curve. It can be observed that TiO₂ paint was able to achieve full nighttime sub-ambient cooling effect. However, it failed to achieve full-daytime cooling as the plot shows that the paint only achieved cooling effect before 11:40am and after 4pm when the solar irradiation was not quite strong. Overall, the TiO₂ nanocomposite paint still shows the potential in achieving better cooling effect even full-daytime cooling. As the high humidity during the experiment period may negatively influence the cooling effects, based on the previous work [13]. Moreover, being able to join Dr.Xiangyu's research provided me a good experience which could benefit my research and design of experiment.

2.2 Colored cooling paints with BaSO₄ nanocomposite

The passive radiative cooling can be efficiently achieved with a dual-layer device with high reflectance of solar irradiation in solar spectrum on the top layer and strong emittance in the transparent portion of the atmosphere by the bottom layer, referring to Dr. Huang and Dr. Ruan [4]. However, the main focus of this work is on the investigation of single layer radiative cooling performance by embedding BaSO₄ nanoparticles in acrylic matrix. In the previous work of our

group, we were actually able to achieve full daytime sub-ambient cooling with BaSO₄ nanocomposites. Standing upon this great success, we decided to push this study one step further to search for the possibility of colored BaSO₄ cooling paint. Same as the TiO₂ nanoparticle composite, the particle size of BaSO₄ nanoparticles is selected to be approximately 500nm as well.

2.3 Fabrication of colored cooling paints

Beginning with the fabrication of colored BaSO₄ paints, the amount of acrylic to be used as the matrix in the composite is controlled to be around 3g. In order to obtain exact amount of acrylic wanted, the utilization of an electronic scale becomes essential. As shown in the Figure 5 below, a paper cup is placed on the scale initially and then tared. So that when the acrylic is added into the paper cup, the cup body weight will not have an influence on weighing acrylic. Toluene as a widely used solvent is employed in this case. The mass ratio between acrylic and Toluene needs to be 1:4 to ensure that the acrylic can be perfectly dissolved in the solvent. As the density of Toluene is $0.87\frac{\text{g}}{\text{cm}^3}$, 12g of Toluene according to the mass ratio thus converts to the requirement of 13.79mL of Toluene. As we always add a little bit more acrylic in the paper cup in case of the mass loss during the experiment, the actual amount of acrylic weighted is usually 0.1g~0.2g greater than the standard 3g. Therefore, the actual volume of the Toluene obtained is set to be 14mL.

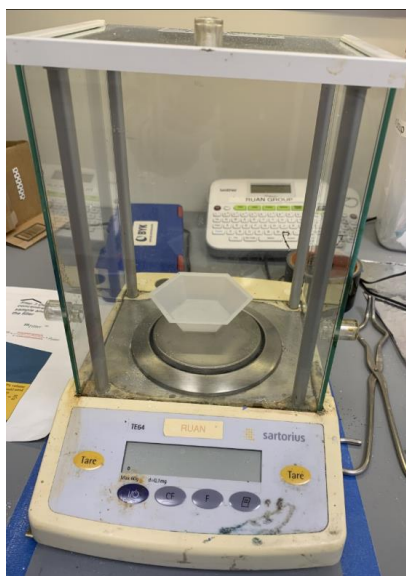


Figure 5. Electron Scale

Then the acrylic can be dissolved into the Toluene, but it needs to be noticed that Toluene must be transferred into the container before acrylic can be dumped into the container. Otherwise, acrylic will deposit at the bottom of the container. In this situation the acrylic deposit will need to be break up and washed out by solvent or it will affect the following fabrication. Next step is to determine the amount of BaSO₄ and color pigments to be embedded as fillers in the acrylic matrix. The mass ratio between the BaSO₄ and color sample is determined to be 5:1, while the volume percent of the fillers is determined to be 60%. It means $\frac{V_{\text{BaSO}_4+\text{color}}}{V_{\text{acrylic}}} = \frac{6}{4}$. Before employing the design of 60% volume percent, we also tried 50% as well as 70% but neither of the samples could meet the specification. The viscosity of 50% volume percent samples became too high and could not form a coating with uniform thickness. Additionally, it has too much of transparency, which will fail to reflect solar irradiation as much as possible. For the 70% volume percent samples, BaSO₄ and color pigments were not able to be dissolved into the solvent as it may exceed the solvent capacity. Continuing in fabricating the composite, Branson Digital Sonifier was utilized in order to fully mix the matrix and fillers together and it could also be utilized to help acrylic dissolve in the Toluene. Similar to how we determined the volume percent, the mass ratio between BaSO₄ and the color sample was also determined after several trials in the experiments. Figure 6 shows the sonifier driving machine and the frame setup including the holder of the probe. The probe shown in Figure 6(a) is capable of vibrating at high frequency and thereby facilitating the dissolving process of acrylic in the solvent or the mixing of BaSO₄ and color pigments in the acrylic-Toluene liquid. We commonly only need 25% of the total power output otherwise the vibration will cause the temperature to increase greatly, which will damage the nanostructure of the acrylic. To prevent from the mixture being over warmed, the water bath method was employed by placing the container inside the square metal case filled with cold water shown in Figure 6(a). That way, the container can be constantly cooled down by the water during the mixing process. We also set the sonifier to rest for 60sec each time after running for 40sec and the total running time for the sonifier is usually set to be 6min. If the acrylic is fully dissolved in the Toluene, which should be visually clear like water, a 6min run of the sonifier can already provide us a well-mixed paint. The last step is to carefully pour the paint on plastic film or glass and let the paint spread evenly. Then we utilized the tool shown in Figure 7 to push across the surface of the spread paint so that all the paints would be maintained at the same thickness.

Since we would also like to study the optical properties of the color pigments in the matrix, we fabricated another group of the color paints with color pigments only. The volume percent of color pigment is determined to be 30%, which is the result after several trials. We tried to make paints with 60% volume percent color pigments, but the finished paint could not be conserved very long. When we measure those paints, they already peeled off from the plastic films. The volume percent of 30% of color pigments provides us the most sustainable paints. Moreover, the volume percent of color pigment is not significant in the paint optical properties. Therefore, with similar operation as how we made the paint added with BaSO₄, we made the color pigment only paints. The thickness of these color pigment only paints is the same as the paints with both color pigment and BaSO₄.

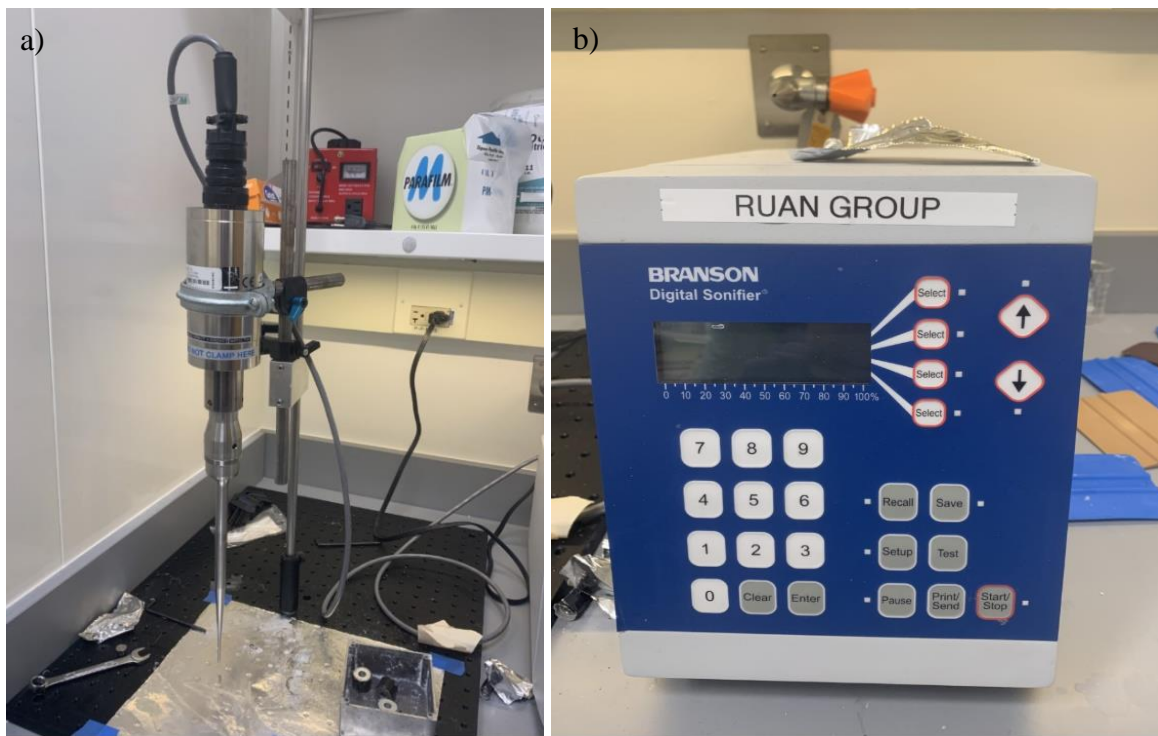


Figure 6. a) Probe of Sonifier and the holder. b) Sonifier driving machine



Figure 7. Tool used in controlling thickness

The color pigments material used in making color paints are shown in Table 1. Color paints materials

Table 1. Color paints materials

	Material name
Light Green	Hydrated Iron Potassium Silicate (Glauconite)
Yellow	Iron Oxide Hydroxide ($\text{Fe}(\text{OH})_3$)
Green	Chromium(III) Oxide (Cr_2O_3)
Blue	Cobalt Zinc Aluminate ($(\text{Co,Zn})_2\text{Al}_2\text{O}_4$)

2.4 Methodology of measurement

2.4.1 Introduction of Spectrometer

Lambda 1050 can characterize UV/Vis/NIR properties across the spectral range of from 200nm to 2.5 μm . It is equipped with a visible lamp and an ultraviolet lamp as the default light sources. In our design of experiment for measuring the reflectance to solar irradiation, we would only need to have the wavelength up to 2.5 μm . Lambda1050 has UV/Vis resolution of 0.05nm when the NIR resolution can reach up to 0.2nm. Therefore, as an industrial standard spectrophotometry, Lambda 1050 was accurate enough and could meet all our needs. The approach it measures reflectance and transmittance is by allowing the light to enter the integrating sphere which can be seen in Figure 8(c), the black chamber that is on the right of the picture.

By placing our color paint samples in the front of the integrating sphere, we can measure the transmittance of samples. The other way around, when the reflectance needs to be measured, color

samples are placed at the back leaving the front empty. The data collected could be saved in the program and plotted with Matlab.



Figure 8. a) Spectrometer Lambda1050. b) The back. c) Inside

2.4.2 Outdoor experiment setup for colored cooling paint

The outdoor experiment was set up on the roof top so that the direct sunlight was secured. With the thermal couple embedded below the color paints, we could record the temperature data during the experiment time period. All the plastic holders were transparent so that they would not have any influence on the reflection of color paints. Side walls of these holders were low enough to just overtop the surface of these paints. Therefore, we can assume that the sunlight can be fully received by paints from all the directions and angles. After finishing the experiment, we could estimate the cooling power of color paints based on the collected temperature data. According to the same model we used in the calculation of cooling power of TiO_2 paints, we should be able to estimate either partial or hopefully full daytime sub-ambient daytime cooling power. The same model could

be applied because there were only minor changes to the variables shown in *Equation 1*. The results of outdoor experiment should provide us a clear image of color paints radiative cooling performance.

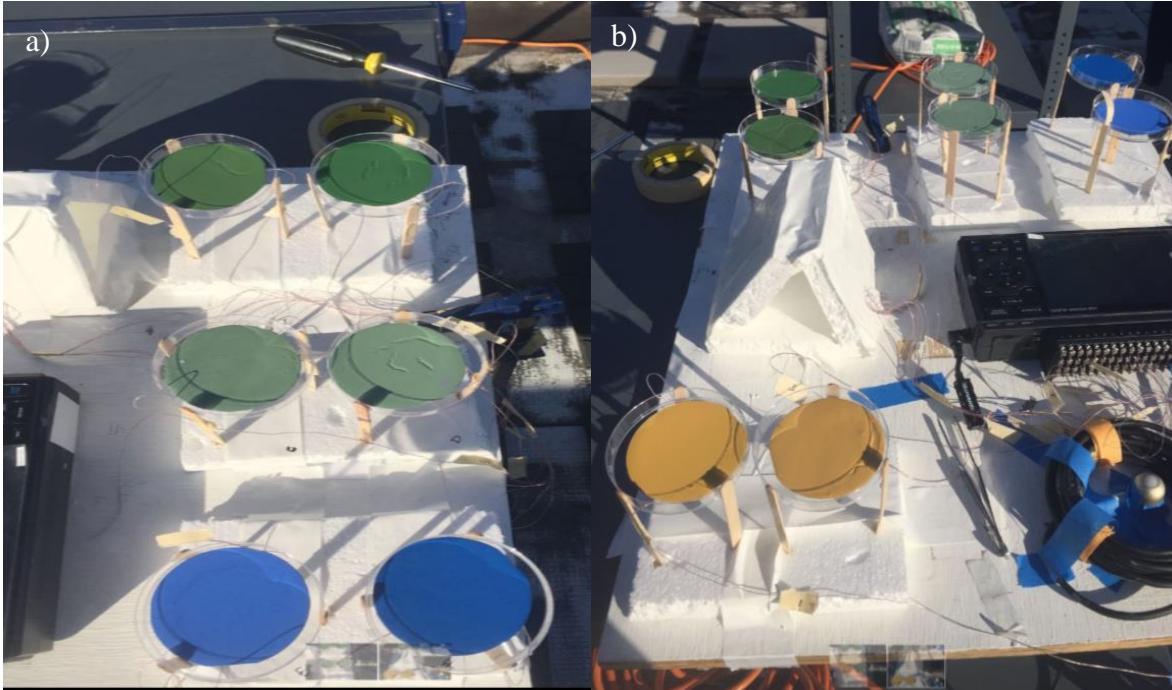


Figure 9. Outdoor experiment setup

2.5 Experimental results

2.5.1 Indoor Spectrometer test result

As we have fabricated color cooling paints with the color of Light Green, Yellow, Green, and Blue, indoor measurements with Perkin Elmer Lambda 1050 UV-Vis-NIR were conducted. The radiative properties of color paints are recorded and plotted with Matlab. The measurement results will be shown and discussed below. Overall, the color cooling paints show good potentials in radiative cooling except the absorption to UV cannot be handled yet. Also, we expected the color cooling paints fabricated to achieve as much of the reflectance as possible and maintain a low absorptance. However, it was hard to achieve because some absorption has to occur to show color. Therefore, we primarily compare our colored cooling paints with commercial colored paints with

the same colors. Meanwhile, we studied the optical properties of color pigment only paints and we can thus learn the strength and weakness of every color paint.

Figure 10 below shows the result of the reflectance of Light Green paints. As a comparison, the performance of commercial paint is included in the plot as well, represented as the black curve. It can be observed that, Light Green color-pigment-only paint (paint embedded with color pigment only) shows relatively low reflectance in the solar spectrum. Commercial paint obviously performs better in reflecting solar irradiation than the Light Green color-pigment-only paint. In contrast to the Light Green color-pigment-only paint, a tremendous improvement in the reflectance can be observed when the paint is also embedded with BaSO₄ nanoparticles. It proves that embedding BaSO₄ nanoparticles in the paint has great potential in radiative cooling as it surpasses commercial paint in this case. Moreover, BaSO₄ is fairly cheap and color paint mixed with BaSO₄ can also be a great application for commercial use. Then, a local reflectance peak can be observed at around 0.58μm in the Light Green color-BaSO₄ paint (paint embedded with color pigment and BaSO₄ nanoparticles) curve. According to solar irradiation distribution graph previously shown in Figure 1. a) Solar irradiation and distribution. b) Transmittance in the sky window, a large portion of solar irradiation comes in the visible range and the peak happens to be around 0.5μm and 0.6μm. Therefore, a strong reflection within this wavelength range is a sign of good potential in being used as a radiative cooling paint.

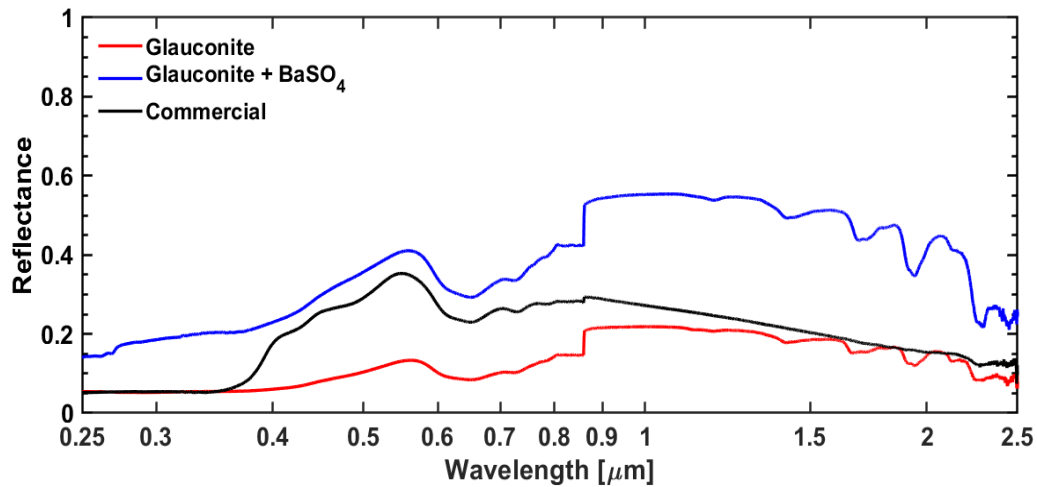


Figure 10. Spectral reflectance of the Light Green paints.

The transmittance curves of Light Green paints are shown in Figure 11 below. After measuring both of the reflectance and transmittance of the paints, we should be able to estimate the absorptance. With the requirement of high reflectance and low absorptance in the solar spectrum, whether the paint can meet the specification can be determined according to the two plots. It can be observed that though the Light Green commercial paint only has a peak reflectance of around 0.3, the transmittance is still too low to be measured. This indicates that it is very absorptive at all the wavelength in solar spectrum. Combining the result shown in the reflectance plot, the ineffectiveness of commercial paint actually supports liability of our results as the commercial paints are not specifically made to own the properties of radiative cooling. Then it can be noticed that the Light Green color-pigment-only paint has much higher transmittance than the Light Green color-BaSO₄ paint over all the wavelength in the solar spectrum. High transmission is not desired if the paint is to be used on an absorptive substrate since the heat will eventually be absorbed by the substrate. Our paint shows higher solar reflectance which is promising.

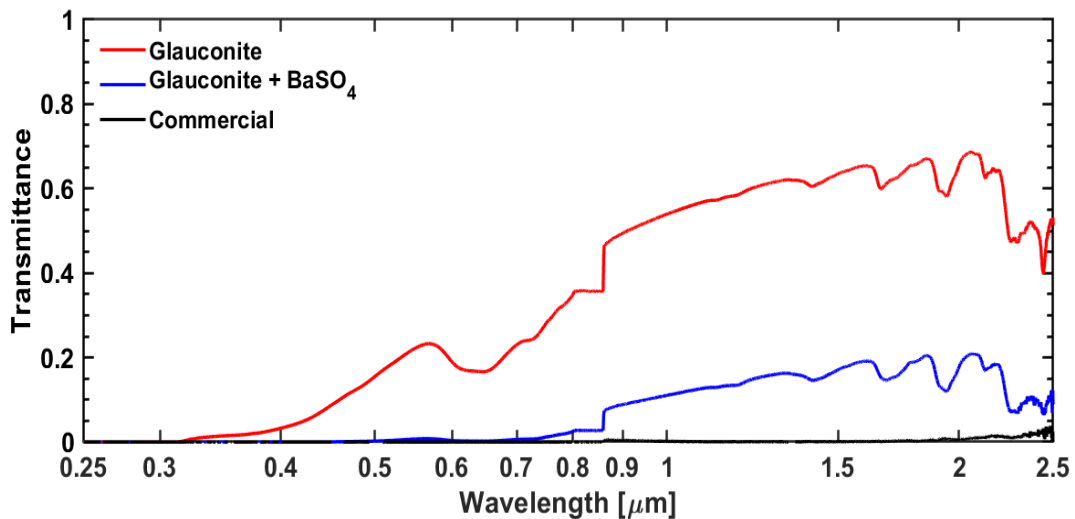


Figure 11. Light Green color paints plot of transmittance

The next color paint we measured is Yellow and the plot of reflectance is shown in Figure 12 below. Similar to Light Green plots, the optical properties of commercial Yellow color paints are included in the plots as well. The rest of color paints plots will be shown with the same pattern. In the reflectance plot, it can be observed that the commercial paint has pretty impressive reflectance

in the range from 0.6 μm to 1.6 μm . For a large portion of this range, commercial paint even has better reflectance than the Yellow color-BaSO₄ paint. Also, the Yellow color-pigment-only paint does not have as high reflectance as the Yellow-BaSO₄ paint does. Considering the same result in the comparison between Light Green color-pigment-only paint and Light green color- BaSO₄ paint, this could be a strong support to our decision of embedding in BaSO₄ nanoparticles to color paints. We will further validate this result with the measurement results from other color paints later. With a rapid increase in reflectance from wavelength of 0.4 μm to 0.7 μm , both commercial Yellow color paint and the color-BaSO₄ paint meet our expectation for high reflectance.

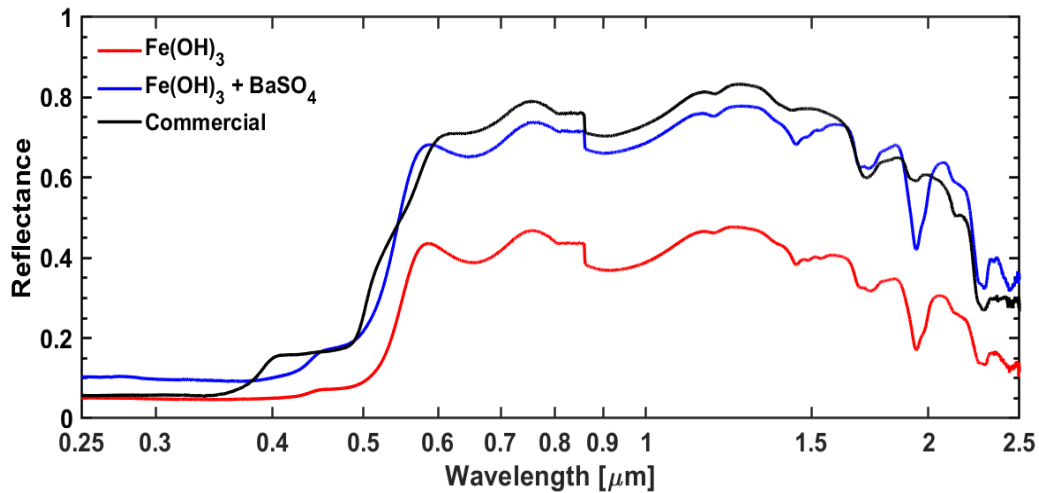


Figure 12. Yellow color paints plot of reflectance

Through observing the Yellow color paints transmittance plot shown in Figure 13, we notice that Yellow color-pigment-only paint still has a higher transmittance in than Yellow color-BaSO₄ paint. Therefore, it may not be a coincidence to have larger transmittance and smaller reflectance for the Light Green color-pigment-only case and this phenomenon is not beyond expectation. As the paints are all at the same thickness regardless of whether added with BaSO₄ or not. Therefore, the density of particles in the paints will become the determining factor. BaSO₄ can provide a great enhancement in reflectance, however, it will increase the density of particles in the matrix and in turn reduce the transmittance of paints. After combining the results in reflectance plot and transmittance plot, we can observe that the absorptance of Yellow color-BaSO₄ paint is low enough

to reach our expectation. Where the low absorptance is largely because of the high reflectance and we are quite satisfied with the performance of Yellow color-BaSO₄ color paint.

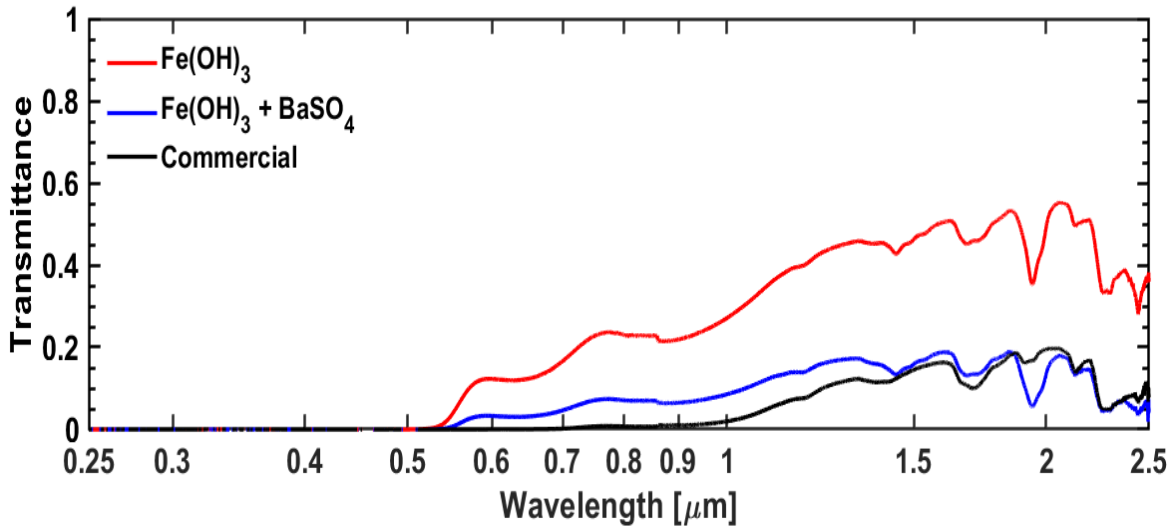


Figure 13. Yellow color paints plot of transmittance

The next color we chose to be fabricate as color cooling paint is Green and the measurement results of Green color paints are shown in Figure 14 below. In the plot of reflectance, commercial paint tends to have higher reflectance only in a short range between 1μm and 1.5μm wavelength. The reflectance before 0.9μm wavelength is unsatisfactory, which will have a negative impact in the radiative cooling performance. Looking at the Green color-BaSO₄ paint we fabricated, the overall trend of the reflectance is quite similar to the Green color-pigment only paint. Therefore, we can now confirm that the addition of BaSO₄ is an enhancement to the original color pigment in the reflectance without changing the color. Then, In the case of Green paints, BaSO₄ still shows a considerable improvement in the reflectance. As in the Green color-pigment-only paint curve, the reflectance is around 0.55 in the wavelength range of 0.8μm to 2.2μm. When added with BaSO₄, the color cooling paint reflectance is improved by almost 0.1, to approximately 0.65. However, the overall reflectance of Green color cooling paint is not as impressive as the Yellow color cooling paint. There are only two insignificant local reflectance peaks at wavelength of around 0.42μm and 0.55μm.

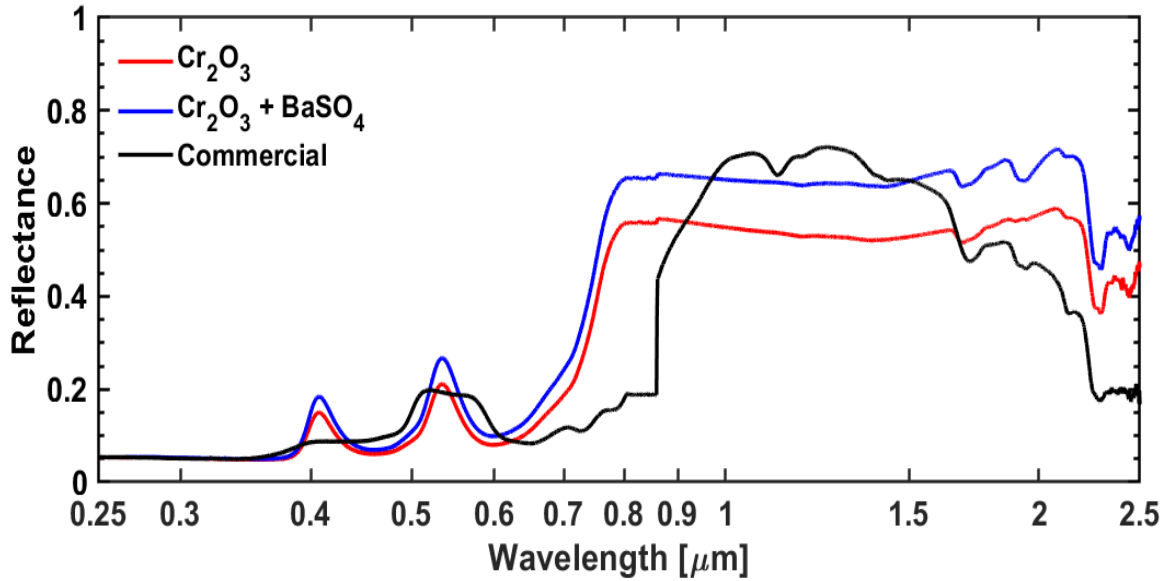


Figure 14. Green color paints plot of reflectance

Then the Figure 15 below shows the transmittance plot of the Green color paints. Different from the previous two commercial color paints, the Green color commercial paint has the lowest transmittance in all the wavelengths. Transmittance of commercial paint only happens after the wavelength of 0.9 μ m, within the wavelength range where the reflectance of commercial paint decreases gradually. With nearly negligible transmittance in UV and visible range, the lack of high reflectance within the same wavelength range can make the absorptance incredibly high. Moreover, as observed from the Green paints transmittance curves in Figure 15, the transmittance for both color-pigment-only and color-BaSO₄ paints are trivial. It will lead to the result that both of the color paints are very absorptive in the wavelength range from 0.25 μ m to 0.8 μ m, except for the wavelength where the two local reflectance peaks occur. Beyond the 0.7 μ m wavelength, the absorptance of Green color paints can be relatively low because of the constant high reflectance in the rest of the wavelength range. The Green color- BaSO₄ paint is able to meet the specification of high reflectance and low absorptance in a wide range of NIR. Our design shows better potential than commercial paint in radiative cooling.

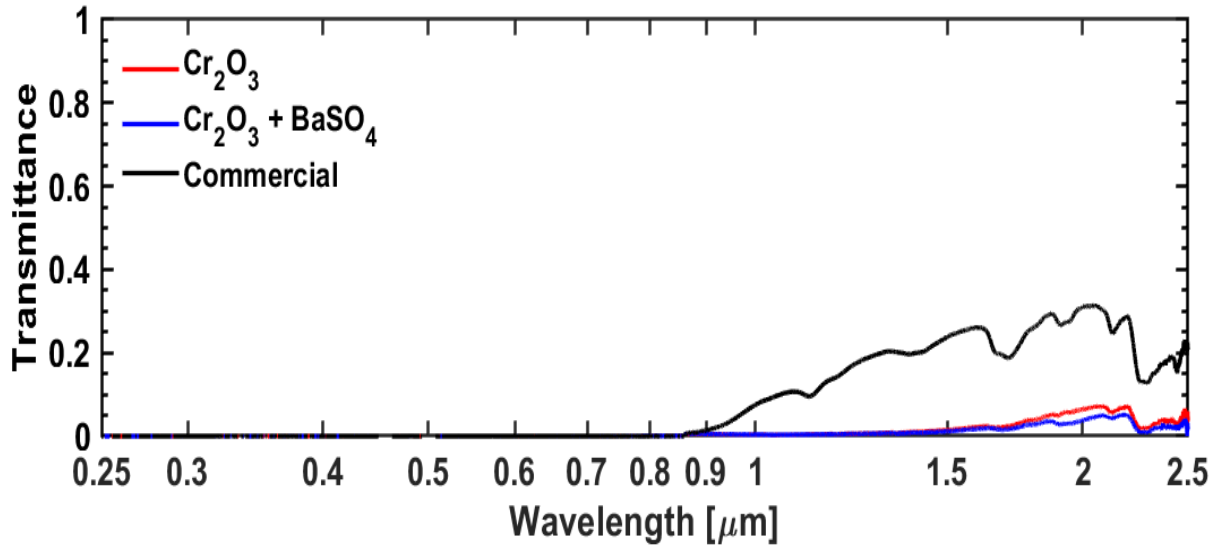


Figure 15. Green color paints plot of transmittance

The last color we chose to include in the design of color cooling paint is Blue. From the reflectance plot of Blue color paints shown in Figure 16 below, it can be observed that the reflectance of commercial Blue color paint has a local reflectance peak at around $0.45\mu\text{m}$ wavelength, which lays within the visible range. Followed with a valley from $0.55\mu\text{m}$ to $0.65\mu\text{m}$, the reflectance jumps to around 0.8 in the wavelength range of $0.7\mu\text{m}$ to $1\mu\text{m}$. Then the reflectance remains constant till $1.5\mu\text{m}$ wavelength and drops gradually after that. Comparing to the commercial paint, Blue color-pigment-only paint has similar local peak of reflectance in the visible range. Then in the NIR, Blue color-pigment-only paint has a valley between $1.2\mu\text{m}$ and $1.5\mu\text{m}$, where the reflectance is close to zero. As a result, it may not be able to reflect much of solar irradiation just according to the result from the spectrometer measurement. The situation becomes better when BaSO₄ is added into the paint, as the local reflectance peak in the visible range is improved to 0.55 . The improvement from BaSO₄ is very impressive to us and Blue color-BaSO₄ paint so far provides us the second-best reflectance in the visible range. The Blue pigment does not show good enough reflectance in visible range while the addition of BaSO₄ increases the reflectance tremendously. We believe that Blue color paint should be granted good radiative cooling potentials after embedded with BaSO₄ nanoparticles

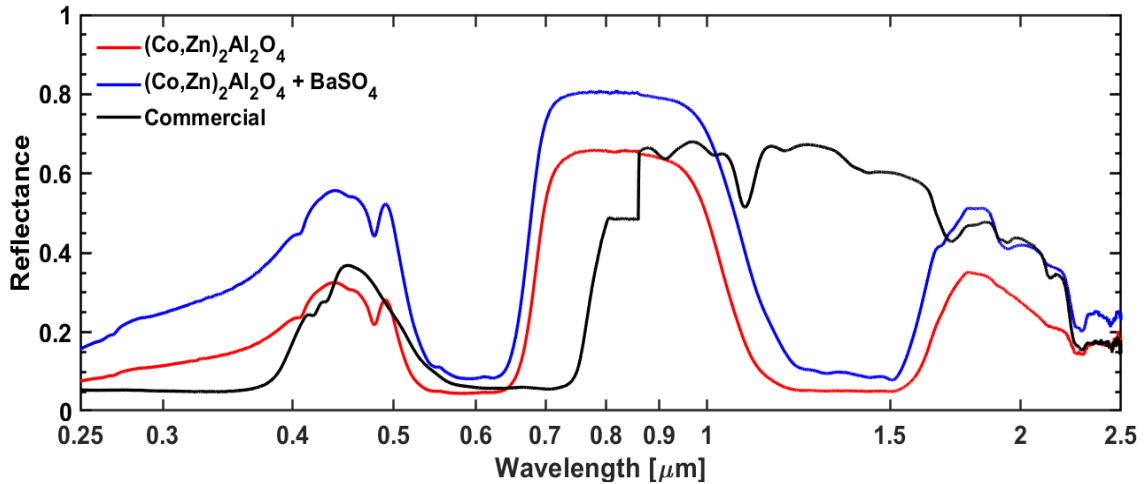


Figure 16. Blue color paints plot of reflectance

Figure 17 below shows the transmittance of the Blue paints. Commercial Blue paint starts to show transmittance from wavelength of $0.7\mu\text{m}$. When considering the reflectance curve, commercial Blue paint has pretty low absorptivity from $0.7\mu\text{m}$ to $2.5\mu\text{m}$ wavelength. Comparing to the commercial paint, our Blue color-BaSO₄ paint has higher absorptance from around $1.2\mu\text{m}$ to $1.6\mu\text{m}$. Since Blue paints all show extremely low transmittance in the visible range, better reflectance performance of Blue color-BaSO₄ paint therefore results in lower absorptance. As we already learned from the previous three different color paint results, the better radiative performance of Blue-BaSO₄ than color-pigment-only paint is within the expectation.

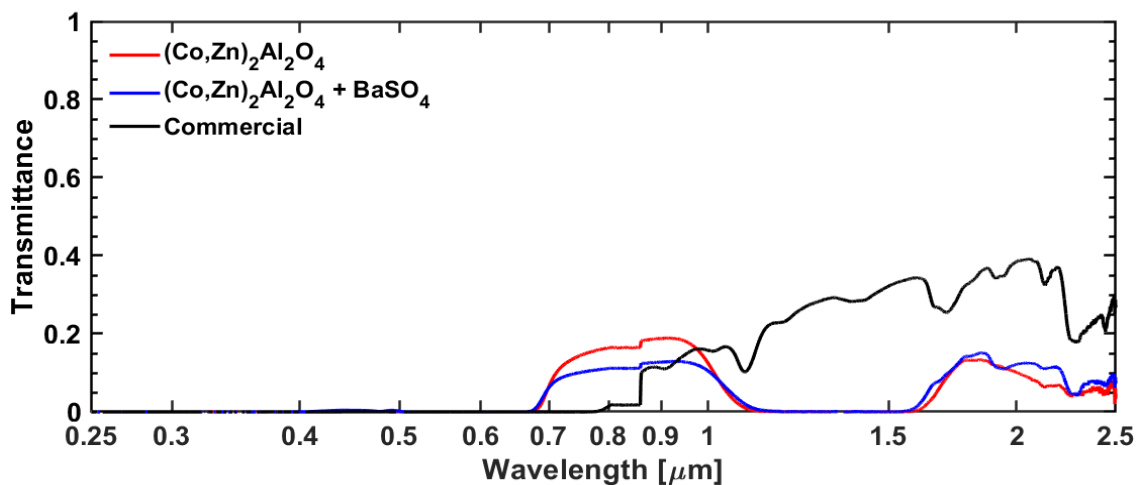


Figure 17. Blue color paints plot of transmittance

In summary, based on the radiative properties of the color pigment only paints, embedding in BaSO₄ nanoparticles has obvious improvement in the reflectance within the solar spectrum for the color paints. At the same time, the absorptance can be maintained at an acceptable level. Therefore, we can expect the color paints embedded with BaSO₄ nanoparticles to show good cooling effect compared to the commercial paints in outdoor experiments. The commercial paints are good comparisons and will thus be tested in the next step outdoor experiment. The performance of each color is shown in the table below. Table.2, Table.3, Table.4, Table.5 will show the color paints comparisons only among the same color. The level of reflectance and absorptance are ranked from low to high. When the same rank appears, it means that the optical properties of the paints are quite comparable with each other.

Table 2. Light Green paints comparison

Color	Paint category	Radiative property	UV	Visible	NIR
Light Green	Light Green pigment	Reflectance	Low	Low	Low
		Absorptance	High	Medium	Low
	Light Green+ BaSO ₄	Reflectance	High	High	High
		Absorptance	Low	Low	Medium
	Commercial	Reflectance	Low	Medium	Medium
		Absorptance	High	High	High

Table 3. Yellow paints comparison

Color	Paint category	Radiative property	UV	Visible	NIR
Yellow	Yellow pigment	Reflectance	Low	Low	Low
		Absorptance	High	Low	Low
	Yellow+ BaSO ₄	Reflectance	High	Medium	Medium
		Absorptance	Low	Low	Medium
	Commercial	Reflectance	Low	High	High
		Absorptance	High	Low	Medium

Table 4. Green paints comparison

Color	Paint category	Radiative property	UV	Visible	NIR
Green	Green pigment	Reflectance	Low	Medium	Low
		Absorptance	High	Medium	High
	Green + BaSO ₄	Reflectance	Low	High	High
		Absorptance	High	Low	Medium
	Commercial	Reflectance	Low	Low	Medium
		Absorptance	High	High	Low

Table 5. Blue paints comparison

Color	Paint category	Radiative property	UV	Visible	NIR
Blue	Blue pigment	Reflectance	Medium	Medium	Low
		Absorptance	Medium	Medium	High
	Blue + BaSO ₄	Reflectance	High	High	High
		Absorptance	Low	Low	Low
	Commercial	Reflectance	Low	Medium	Medium
		Absorptance	High	High	Medium

2.5.2 Outdoor test results of colored paint temperature

The temperature of color cooling paints and commercial paints were recorded and plotted with Matlab. These are all color-BaSO₄ paints as we believed that BaSO₄ would grant color pigment only paints superior improvement in radiative cooling effect according to the spectrometer measurement results. Also, we compared our color cooling paints with the commercial color paints so that we could learn the commercial potential of our color cooling paints. The pink shaded area exhibits the solar irradiation strength within the experiment period. The color cooling paints in the initial experiment on Oct.23rd 2019 were not able to achieve sub-ambient daytime cooling. Moreover, the fluctuations of temperature profiles are fairly intense. Considering the large wind happened on the high roof top, it might have influence on the results. More detailed discussions and thoughts about the experiment results will be shown in the following paragraph.

Figures below show the four different color paints outdoor experimental results. All the curves presented in the Temperature and Solar irradiation plots show the temperature throughout a 10-hour period from 10AM to 8PM. As can be observed in Figure 18, temperature of both paints exceeded the ambient temperature. Therefore, the net sub-ambient cooling power during the daytime turned to be zero according to the equation $h(T_s - T_{amb}) = h\Delta T = \alpha G - q''_{radiation}(T) - \frac{mC_p}{A} \frac{dT}{dt}$ mentioned previously. Since the most significant effect we expected was to surpass the cooling effect of commercial color paint. Though it shows some nighttime cooling, it cannot show distinguished cooling effect compared with the commercial paint according to the temperature curves after 5PM in Figure 18. As the plot of temperature difference between cool color paint and commercial paint in Figure 18 shows, the nighttime temperature difference between the two paints are too small and almost negligible. This phenomenon is not a coincidence, which can also be observed in other color paints outdoor experiment results. Therefore, the emittance of commercial paints and our color cooling paints can be very close. In order to achieve better radiative cooling effect than the commercial paints, trying to achieve partial or even full daytime cooling is a more urgent topic than achieving higher nighttime cooling. Then when considering the temperature difference between Light Green cool color paint and commercial Light Green paint, the temperature difference actually increases with the increases in solar irradiation power. Which is a positive sign that Light Green cool color paint actually has a better performance in reducing the surface temperature than the commercial Light Green paint nowadays. This improvement is very likely brought by the higher reflectance of the color cooling paints because of the BaSO₄ nanoparticles embedded.

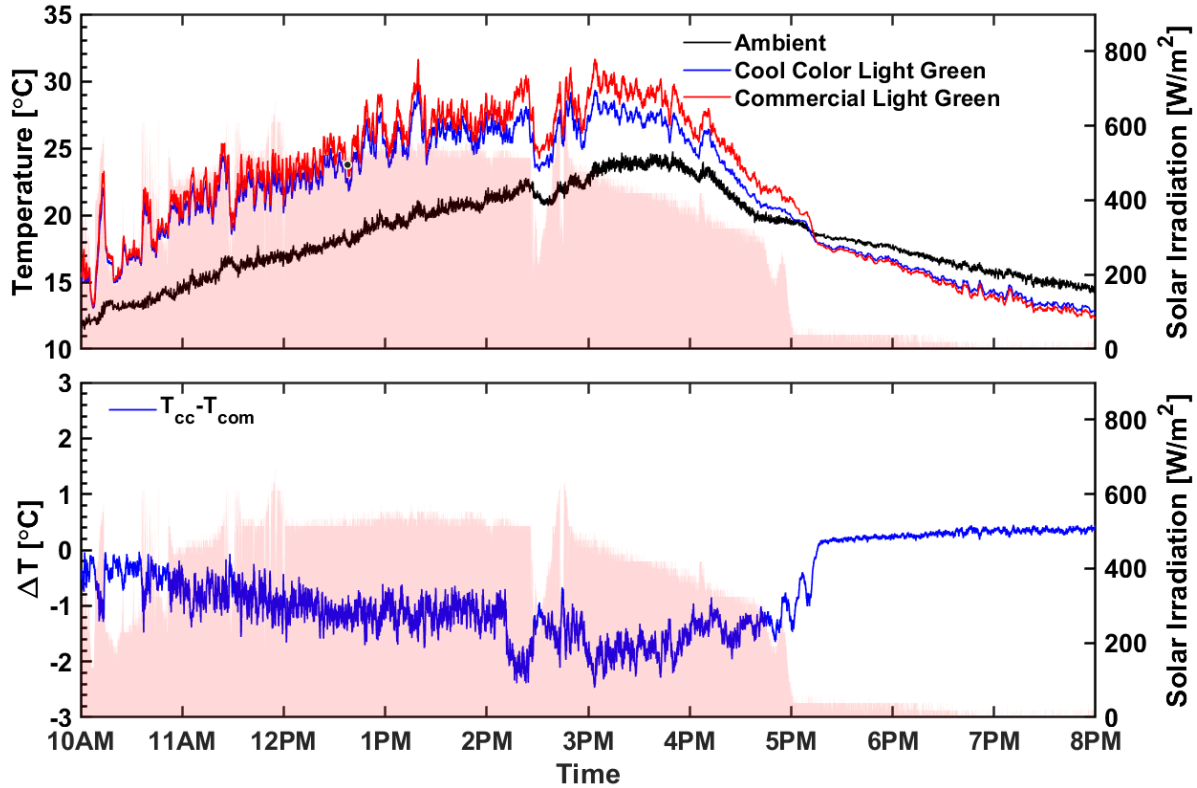


Figure 18. Oct.23rd Light Green color paints outdoor experiment, West Lafayette, IN

Then Figure 19 shows the outdoor experiment results of Yellow Color paints. Same as the Light Green color cooling paint, Yellow color cooling paint did not achieve daytime cooling while achieved some cooling effect during the nighttime. Yellow color cooling paint was expected to provide good cooling radiative cooling effect because of the high reflectance and low absorptance in the solar spectrum according to the indoor measurement. There was some sub-ambient nighttime cooling during the time period of 5PM to 8PM while the solar irradiation got close to zero. Therefore, with higher temperature than the ambient during daytime, we realized that the reflectance of our cool color paint could not reach the threshold of providing radiative cooling effect. The temperature difference between commercial Yellow paint and our cooling paint is quite close compared with the Light green paints. Where the temperature of Yellow color cooling paint is around 1°C lower than the commercial Yellow paint during the daytime while Light Green color cooling paint could reach 2°C lower than commercial Light Green paint. We can probably learn from this result that BaSO₄ has greater improvement in cooling for Light Green color paints comparing to Yellow color paints. However, considering the fluctuations of the temperature

profiles, it can be meaningless to make a judgement based on the results with so many uncertainties. What worth thinking carefully is the influencing factors of the experiment and find possible approaches of improving the accuracy of results.

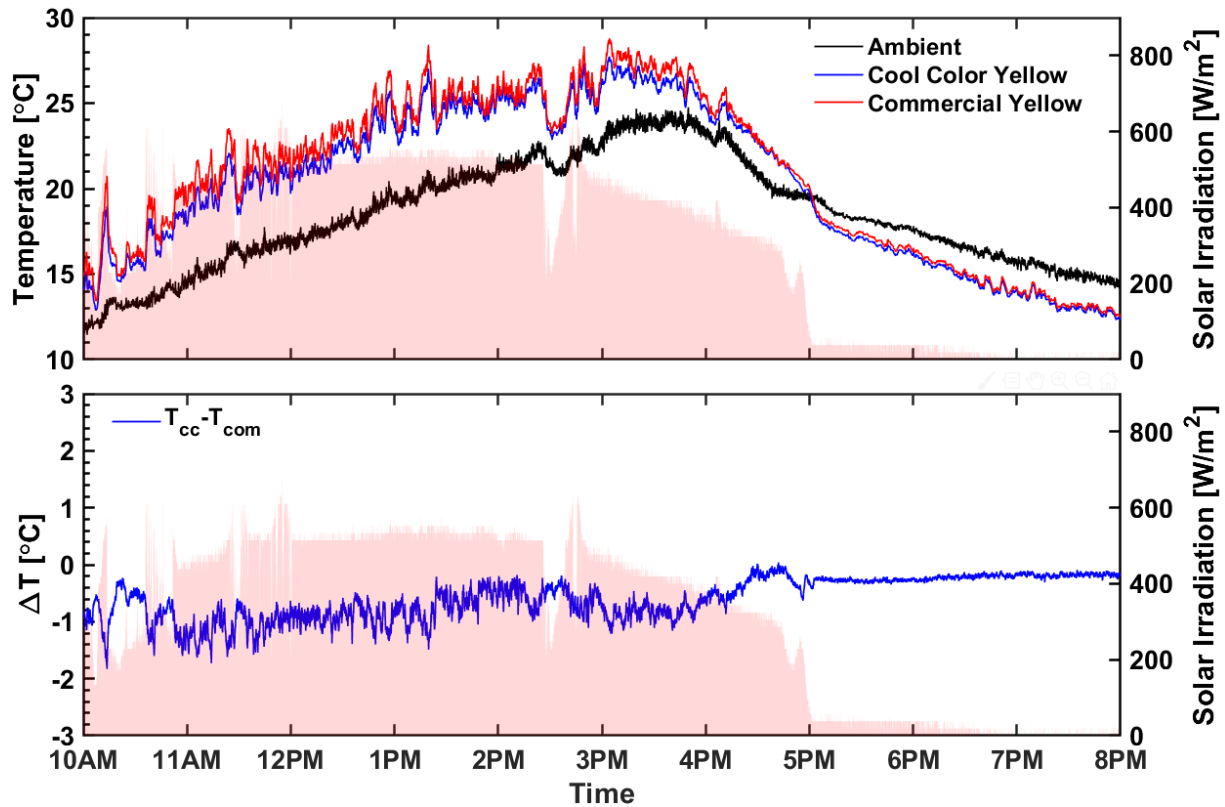


Figure 19. Oct.23rd Yellow color paints outdoor experiment, West Lafayette, IN

The next color paints shown in Figure 20 are Green color cooling paint and commercial Green paint. Green cooling paint still does not show daytime radiative cooling effect according to the temperature profile from 10AM to 5PM. However, it can be observed that both Green color cooling paint and commercial Green paint temperature curves overlap with the ambient temperature curve. It shows a trend that when the solar irradiation grows weaker, it is more likely for the cooling paint to realize sub-ambient cooling effect. It is understandable since lower solar irradiation in turn decreases the total solar reflectance needed. As the reflectance of cooling paints is not ideal for now, it is possible to achieve temporary sub-ambient cooling effect in a day without strong sun light. Looking at the temperature difference curve shown in the second plot of Figure 24, the difference of temperature fluctuates around zero. We expected the cooling paint temperature to be

lower than the commercial paint for every color, however, it seems that by just embedding BaSO₄ nanoparticles as additional filler may not have obvious enough improvements on the cooling effect for Green. At the same time, this could just be a preliminary conclusion and we would further study the potential of Green cooling paints as well as other color paints with more experiments.

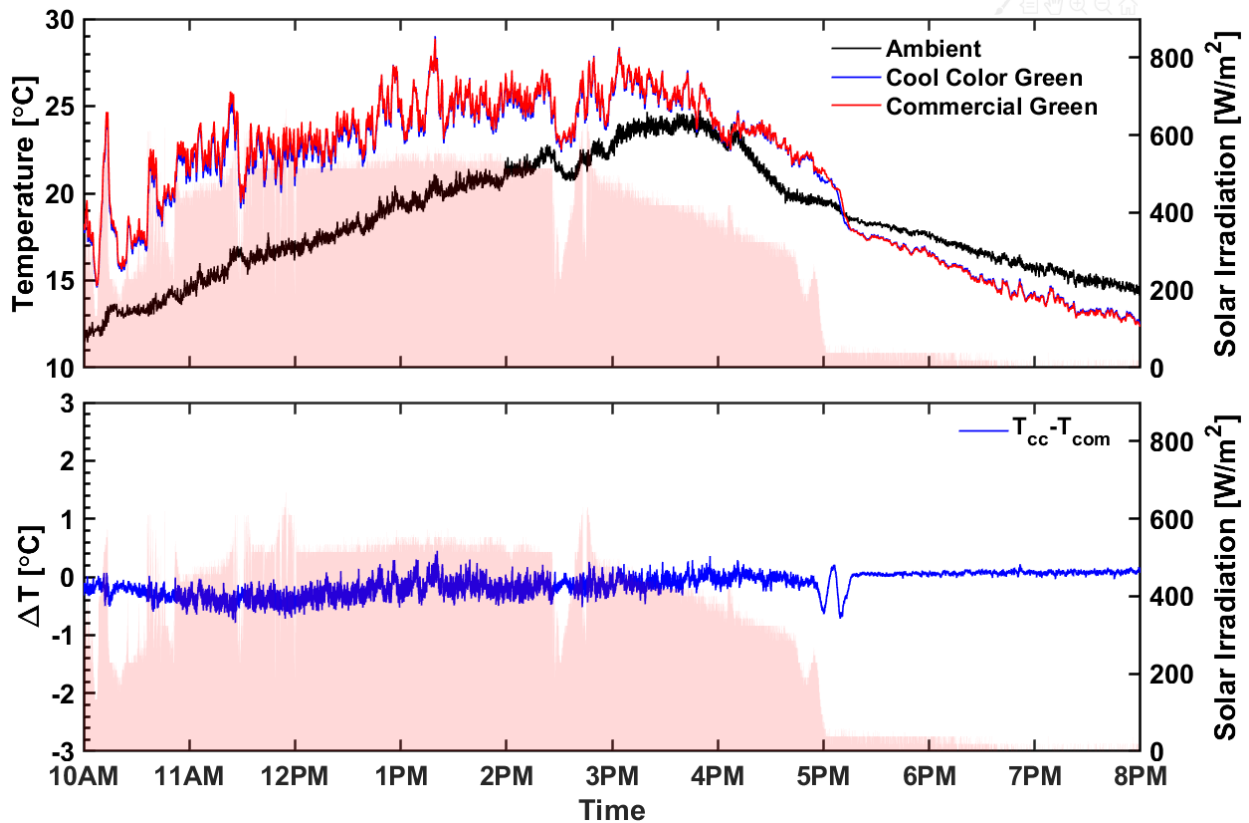


Figure 20. Oct.23rd Green color paints outdoor experiment, West Lafayette, IN

The last color paint presented as Figure 21 is Blue. It shows some nighttime cooling ability, however, we were expecting more. The fluctuation of temperature profile is intense and therefore brings too many uncertainties for us to tell if it has any improvement compared to the commercial Blue paint. In order to exclude the uncertainties from the experiment, we conducted another experiment on Oct.28th 2019. We believed that the intense fluctuations of the temperature profile were caused by the strong wind, which might cause misleading results.

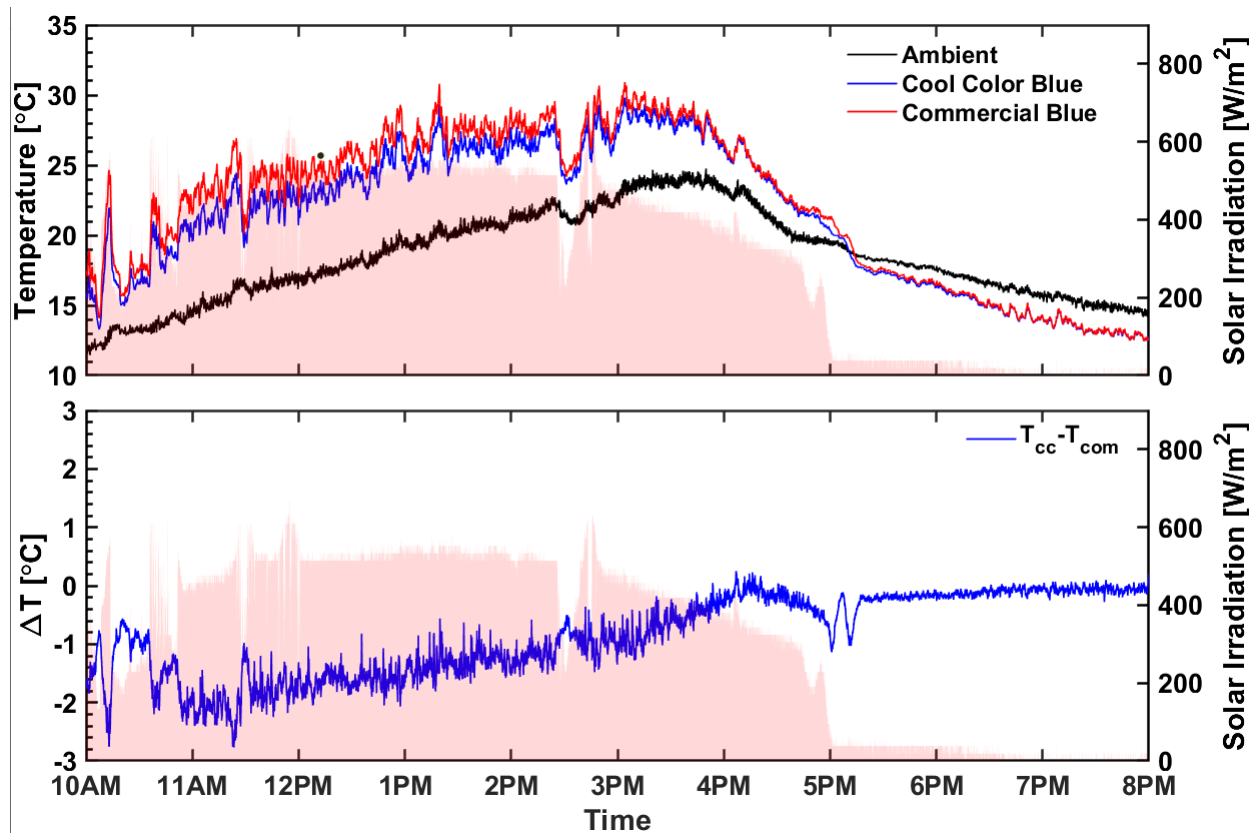


Figure 21. Oct.23rd Blue color paints outdoor experiment, West Lafayette, IN

Therefore, in the second outdoor experiment, we covered the whole setup with visibly transparent plastic film. The plastic film allowed us to secure the direct sunlight and prevent the wind from affecting the experiment. Then, the following figures are the results from the Oct.28th 2019 outdoor experiment.

Results from the second outdoor experiment are shown as following figures. It is quite obvious that fluctuations in temperature profiles are reduced because of the plastic film, so that we should be able to draw some reliable conclusions. Unfortunately, this time our cooling paints still could not provide a daytime cooling and even nighttime cooling. Therefore, it is essential to study how much of improvement in cooling performance that our color cooling paint can bring to the commercial color paint. Overall, a larger temperature discrepancy is shown between color cooling paints and commercial paints in Oct.28th experiment than in the Oct.23rd experiment. However, it can be observed that the color cooling paints not always show lower temperature than commercial paints. In the case of Light Green shown in Figure 22, the cooling paint temperature actually grows

higher than commercial paint from around 12:30PM to 1:30PM when the solar irradiation is at the peak during the day. It probably means that BaSO_4 improves the reflectance and helps with the color paint cooling effect, but this cooling effect fails when the solar irradiation grows to around $600 \frac{\text{W}}{\text{m}^2}$. The sudden increase in the temperature cannot be fully explained based on our current study on colored cooling paints. Then an effective way to estimate the improvement of cooling effect of our cooling paint compared to the commercial paint is by looking at the peak temperature difference in the second plot of Figure 22. The largest temperature difference occurs at around 11:40am, which is a 5°C discrepancy between our colored cooling paint and commercial color paint. Though the sudden temperature jump occurs at around 12:30pm, achieving 5°C below the commercial color paint is still quite an improvement.

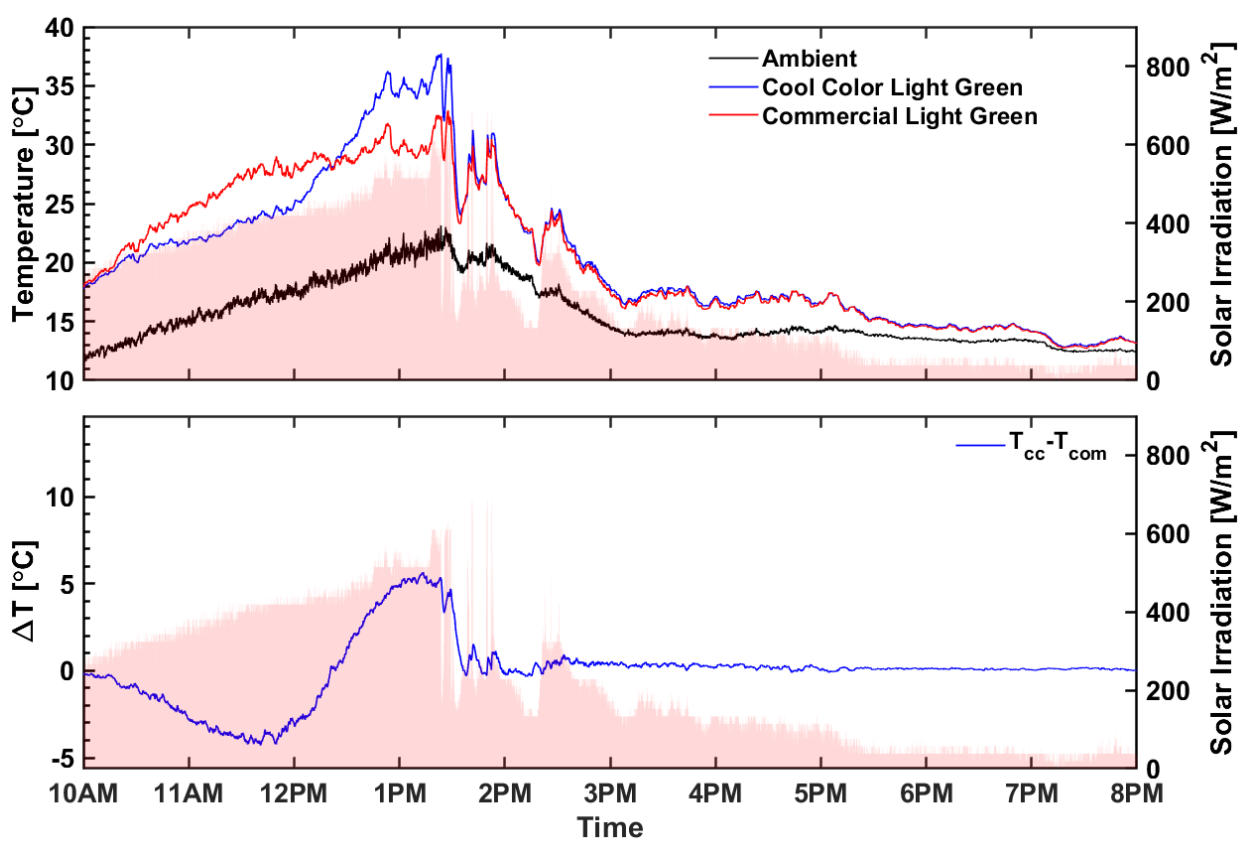


Figure 22. Oct.28th Light Green color paints outdoor experiment, West Lafayette, IN

Compared with Light Green color paints, peak temperature of Yellow color cooling paints and commercial Yellow paints are lower according to Figure 23. Yellow color cooling paint shows 5°C

lower peak temperature than Light Green color cooling paint, while commercial Yellow paint shows 2-3°C lower peak temperature than the Yellow cooling paint. Therefore, Yellow cooling paint shows the better performance in cooling effect while the improvement in radiative cooling is not as good as Light Green cooling paint.

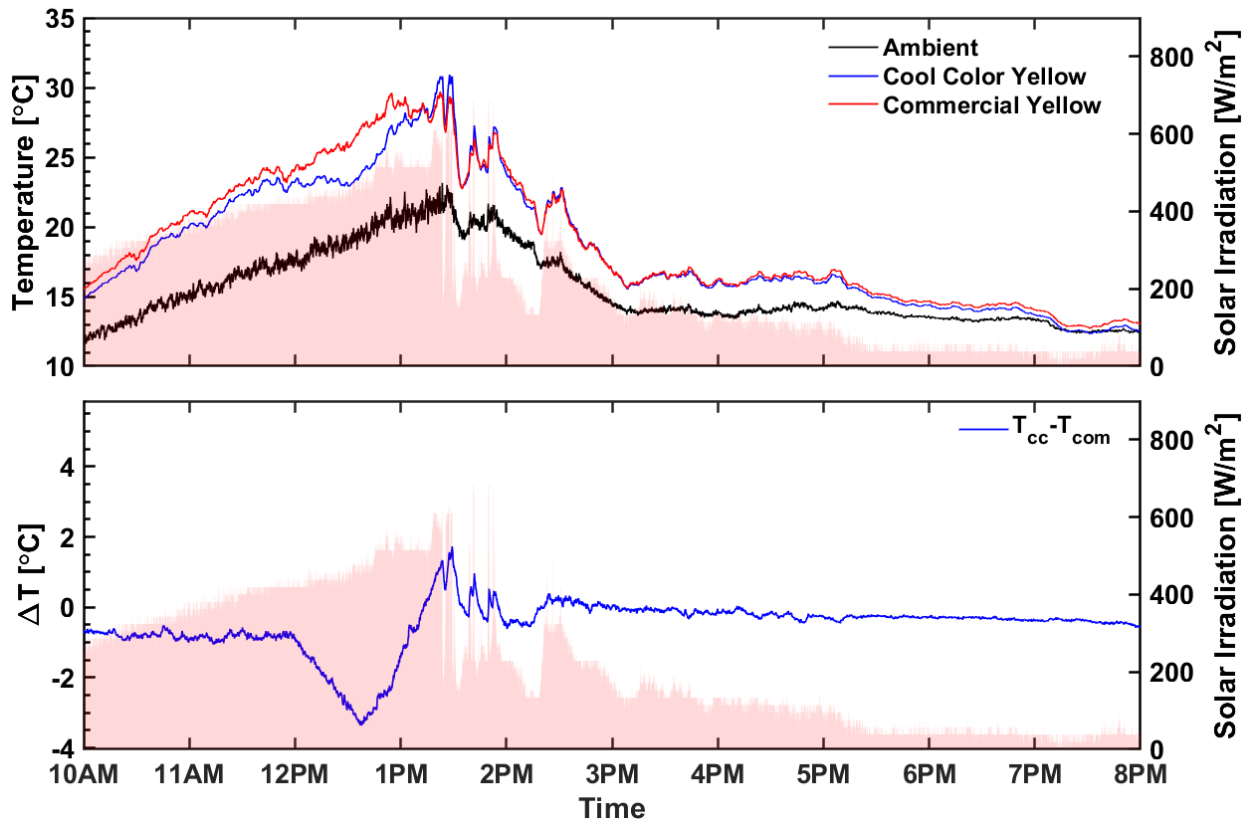


Figure 23. Oct. 28th Yellow color paints outdoor experiment, West Lafayette, IN

For the Green cooling paint, the peak temperature reaches 40°C and the maximum temperature reduction achieved is around 3°C. Different from the previous Light Green and Yellow color paints, it seems that Green cooling paint can always remain a lower temperature than the commercial color paint according to the temperature difference plot. Therefore, we may need more experiments to actually find if this is simply a coincidence or to better understand the reason. If there is really a reason that makes Green special, we may find a way to eliminate the sudden temperature jumps in the other colored cooling paints.

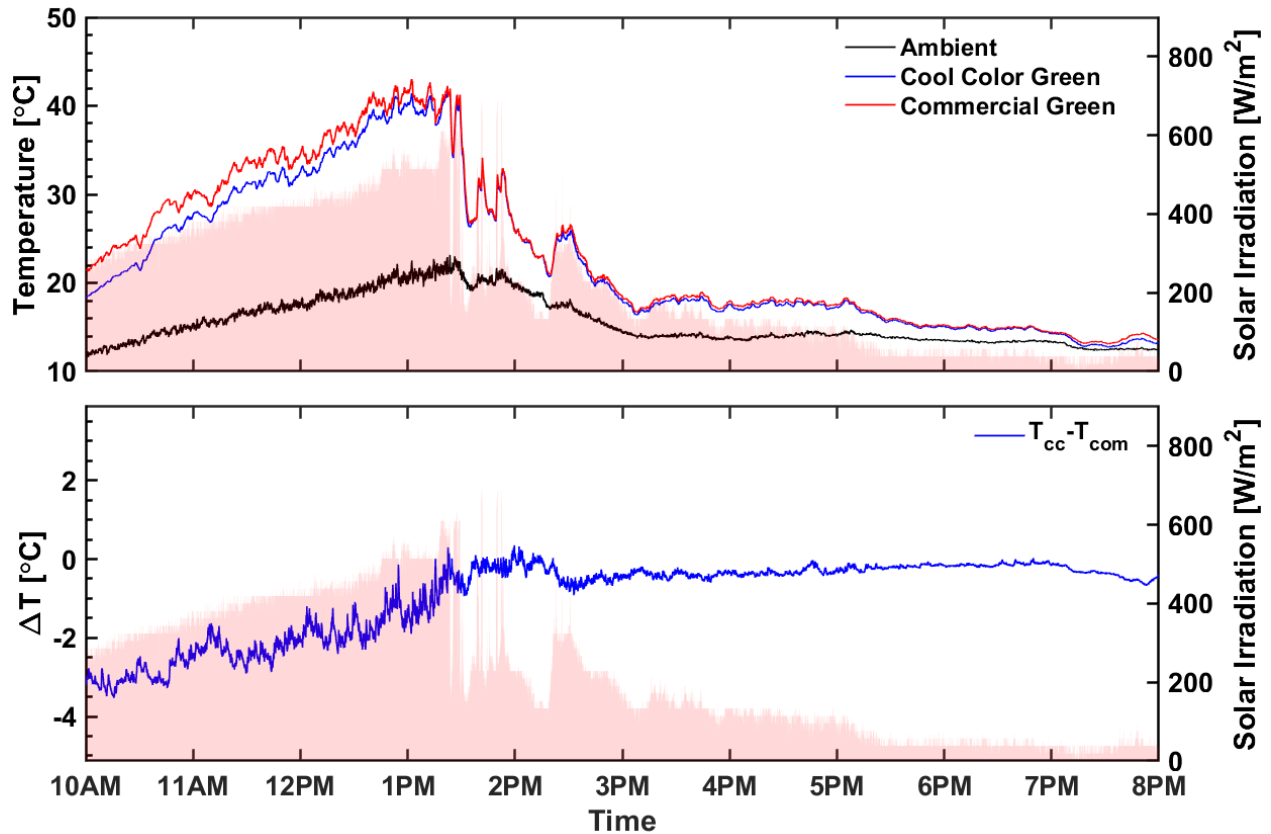


Figure 24. Oct.28th Green color paints outdoor experiment, West Lafayette, IN

Then for the Blue cooling paint, the highest temperature achieved is around 37°C. Then the largest temperature reduction can be observed to be 4°C below the commercial color paint. Therefore, our Blue cooling paint also shows a great improvement in the cooling effect compared to commercial color paint.

In conclusion, all the four colored cooling paints show improvements in the cooling effect. With the purpose of confirming the result correctness, we compared our outdoor experiments with the indoor spectrometry measurements. Larger cooling effect observed in Light Green and Blue cooling paints in outdoor experiment, as they present larger temperature drops compared to Yellow and Green color paints. This result is actually agreed with our experiment results from the indoor measurements. Therefore, with the confirmed correctness of our experiment results, we will make improvements to our colored cooling paints in the future study.

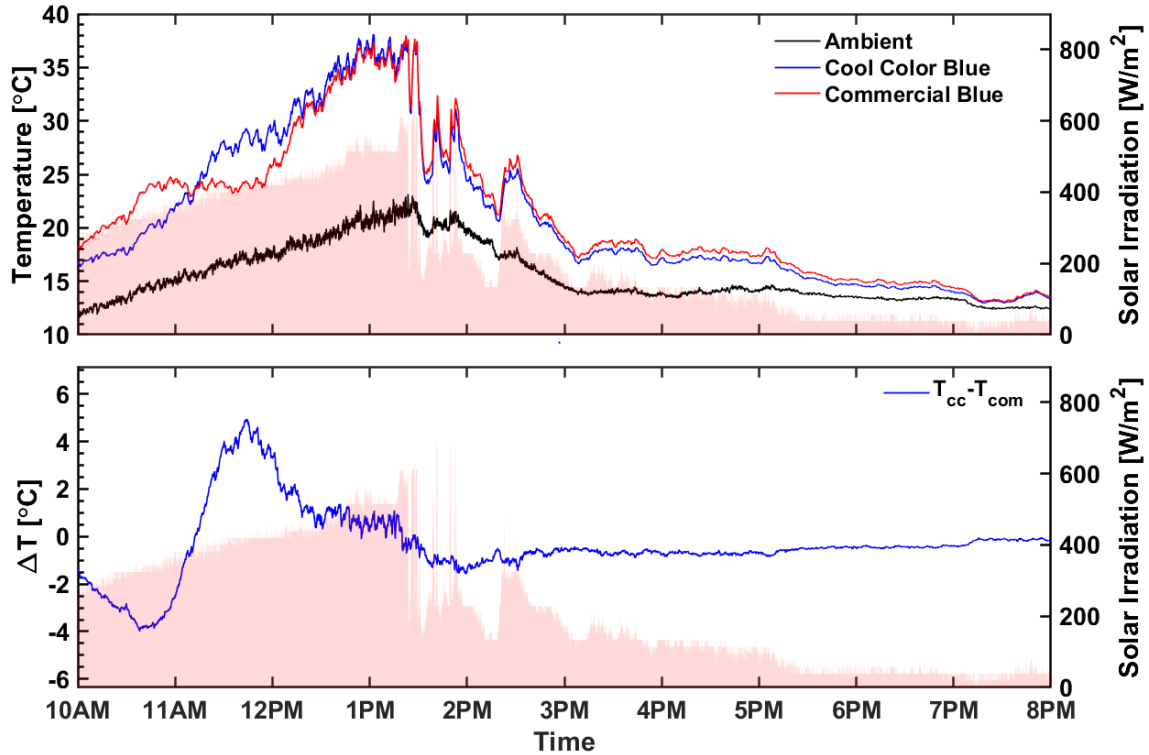


Figure 25 Oct.28th Blue color paints outdoor experiment, West Lafayette, IN

2.6 Further work in optimizing solar reflectance

Because the performance of color cooling paints embedded with BaSO₄ were under the expectation, analysis on the optimum radiative properties of these paints could be a guidance of future study. In order to achieve the best passive radiative cooling effect, the sample paint should achieve high reflectance in the solar spectrum and high emittance in the transparent portion of the atmosphere. Since the nanoparticles in the nanocomposites are responsible for the reflectance in the solar spectrum while the acrylic matrix is responsible for the emittance in the transparent portion of atmosphere. Therefore, analysis would mainly focus on maximizing the reflectance in the solar spectrum by analyzing the particles sizes of nanoparticles and volume fractions.

The first procedure of the optimization work is to construct a quadratic response surface to map the initial design space of three nanoparticle sizes. Two design space sampling routines were used, which is initially mapped by Box and Behnken design and then implemented by the more computationally expensive Full Factorial design. After constructing quadratic response space, the Sequential Quadratic Programming(SQP) algorithm could then be utilized to optimize the design

space variables from the quadratic surface approximation with MATLAB's function `fmincon()`. Then the optimized design space variables can be used to estimate the optimized solar reflectance. The design variables are given by:

$$\mathbf{x} = [r_1, r_2, r_3, vf_1, vf_2, vf_3]$$

,where $r \in [50 \text{ nm}, 625 \text{ nm}]$; $vf \in [1\%, 58\%]$. r represents the particle size and vf represents the particle volume fraction. In this optimization, we are expecting maximized reflectance. Therefore, function $f(\mathbf{x}) = 1-R(\mathbf{x})$ is minimized and $R(\mathbf{x})$ is the reflectance which can be solved with engineering analysis tools. The engineering analysis tools will be introduced in the next section

2.6.1 Analysis tool

The analysis tool used in the optimization process is the combination of Modified Mie Theory(MMT) and Monte Carlo simulations(MC) in the purpose of predicting the total solar reflectance as well as mapping the initial design space. The MMT is responsible for calculating scattering coefficient, absorption coefficient and asymmetric parameter of the composites. These results then will be used as the input parameters for the MC simulations to calculate the reflectance, transmittance, and emittance of the composites.

2.6.2 Modified Mie theory

In this work, the traditional Lorentz-Mie theory is modified to include matrix absorption, multiple particle sizes and dependent scattering effects. The input parameters for MMT are the wavelength (λ), the complex index of refraction of the media (m_{med}), the complex index of the refraction of particles (m_p), particle sizes (d_i) and the volume fractions of each particle (vf_i). After plugging the input parameters into the equations (2) – (8) shown below, the scattering coefficient (σ_T), absorption coefficient (K_T) and asymmetric parameter (g_T) can be calculated.

The scattering efficiency can be calculated with *Equation 2*:

$$Q_{sca} = Z * \sum_{n=1}^{n_{max}} (2n + 1)(|a_n|^2 + |b_n|^2) \quad (2)$$

$$\text{Where, } Z = \frac{\lambda^2}{(2\pi)^2 \gamma |m_{med}|^2},$$

$$\gamma = 2 \frac{1+(\alpha-1)\exp(\alpha)}{\alpha^2},$$

$$\alpha = 4\pi r \frac{\text{Im}(m_{med})}{\lambda}$$

The extinction efficiency can be calculated with *Equation 3*:

$$Q_{ext} = \frac{\lambda}{2\pi^2 r^2} \sum_{n=1}^{n_{max}} (2n+1) \text{Re}\left(\frac{a_n + b_n}{m_{med}^2}\right) \quad (3)$$

The dependent scattering correction is obtained by the *Equation 4*:

$$\eta = \eta_i * [1 + 1.5 * f_t - 0.75 * f_t^2] \quad (4)$$

The scattering coefficient ($\sigma_{s\lambda}$) can then be obtained in *Equation 5*:

$$\sigma_{s\lambda} = \eta \sum_{i=1}^m \pi r_i^2 f_i Q_{sca,i} \quad (5)$$

Next, the extinction coefficient ($\sigma_{T\lambda}$) is obtained by the *Equation 6*:

$$\sigma_{T\lambda} = \sigma_{a,med} + \sum_{i=1}^m \pi r_i^2 f_i Q_{ext,i} \quad (6)$$

Where, $\sigma_{a,med} = \frac{4\pi \text{Im}(m_{med})}{\lambda}$

Therefore, the absorption coefficient ($K_{T\lambda}$) is calculated by *Equation 7*:

$$K_{T\lambda} = \eta(\sigma_{T\lambda} - \sigma_{s\lambda}) \quad (7)$$

In the end, the asymmetric parameter is obtained by *Equation 8*:

$$g = \langle \cos\theta \rangle = \frac{4}{x^2} \left[\sum_{i=1}^m \frac{n(n+2)}{n+1} \text{Re}(a_n a_{n+1}^* + b_n b_{n+1}^*) \right. \\ \left. + \sum_{n=1}^{n_{max}} \frac{(2n+1)}{n(n+1)} \text{Re}(a_n b_n^*) \right] \quad (8)$$

, a_n and b_n shown in the equations above are Mie Coefficients:

$$a_n = \frac{\psi_n(x) m_{med} A_n(y) - m A_n(x)}{\xi_n(x) m_{med} A_n(y) - m B_n(x)}$$

$$b_n = \frac{\psi_n(x) m A_n(y) - m_{med} A_n(x)}{\xi_n(x) m A_n(y) - m_{med} B_n(x)}$$

, where A_n and B_n are : $A_n(z) = \frac{\psi_n'(z)}{\psi_n(z)}$; $B_n(z) = \frac{\xi_n'(z)}{\xi_n(z)}$

, and x, y are the different size parameters: $x = \frac{2\pi r m_{med}}{\lambda}$; $y = \frac{2\pi r m}{\lambda}$

ψ_n and ξ_n are the Riccati-Bessel Functions given by:

$$\psi_n(r) = r j_n(r)$$

$$\xi_n(r) = r j_n(r)$$

The numerical approximation for convergence is given by:

$$n_{max} = x + 4x^{1/3} + 2$$

2.6.3 Monte Carlo method

With the scattering coefficient, absorption coefficient and asymmetric parameter given as mentioned in the previous MMT section, the Radiative Transfer Equation (RTE) can therefore be solved by the Monte Carlo (MC). The RTE is given as shown below:

$$\frac{dI_\lambda}{ds} = k_\lambda I_{\lambda b} - (k_\lambda + \sigma_{\lambda s}) I_\lambda + \frac{\sigma_{\lambda s}}{4\pi} \int_{4\pi} I_\lambda(\hat{s}_i) \Phi_\lambda(\hat{s}_i, \hat{s}) d\Omega_i \quad (9)$$

In this case, an open-source code developed by Want et al. [16] can be used to fulfill the simulation. Since MC is a stochastic process, a large number of photons is required in order to obtain a reasonable result. Therefore, a total of 50,000 photons over 208 discrete wavelengths in the range from 0.25 μm to 2.5 μm should be released in the analysis.

However, this simulation has not been fully conducted yet and it will be our main focus in the future work. We will also look for more optimization algorithms because the current algorithm employed is only second order, which may not be complicate enough to explain the relationships among the variables. In the end, we hope our work in optimizing the color cooling paint solar reflectance can provide a guidance in the fabrication of paints.

3. BIO-INSPIRED RADIATIVE COOLING

3.1 Desert snail

Desert snail is known to be able to survive in the most extreme environments on the Earth. As the surface temperature sometimes can reach as high as 65°C along with the deadly sunlight in the desert, shells of the desert snail therefore should be capable of reflecting a large percent of the solar irradiation to maintain snails body temperature at a safe level. And a picture clearly describes how these shells protect desert snail from being killed by the heat [17].

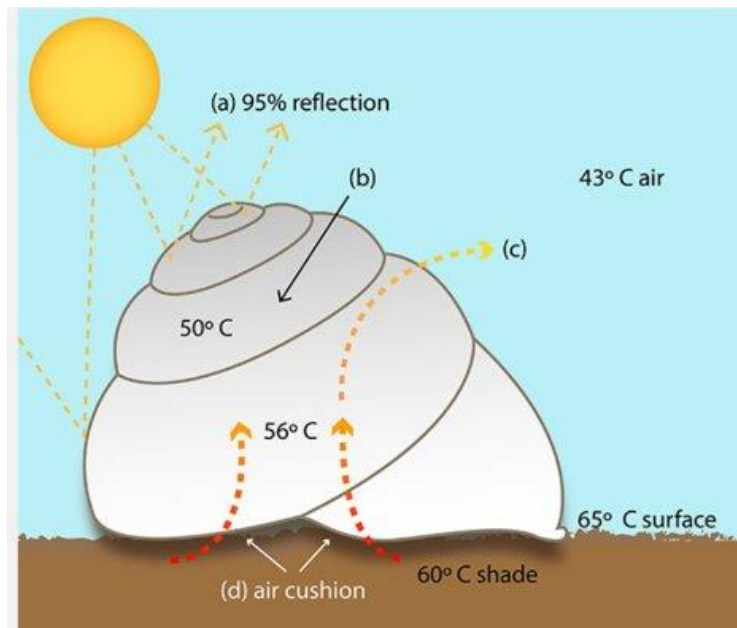


Figure 26. Showcase of Desert snail shell in transferring heat [17]

Through studying the desert snail shell, we expect to understand the key for such a high reflectance to the solar irradiation. However, a clean desert snail sample is hard to be accessed and we have to find a replacement as the research target. Seashells are then studied as an alternative to desert snail shells because of the similar compositions in the shells.

3.2 Seashell

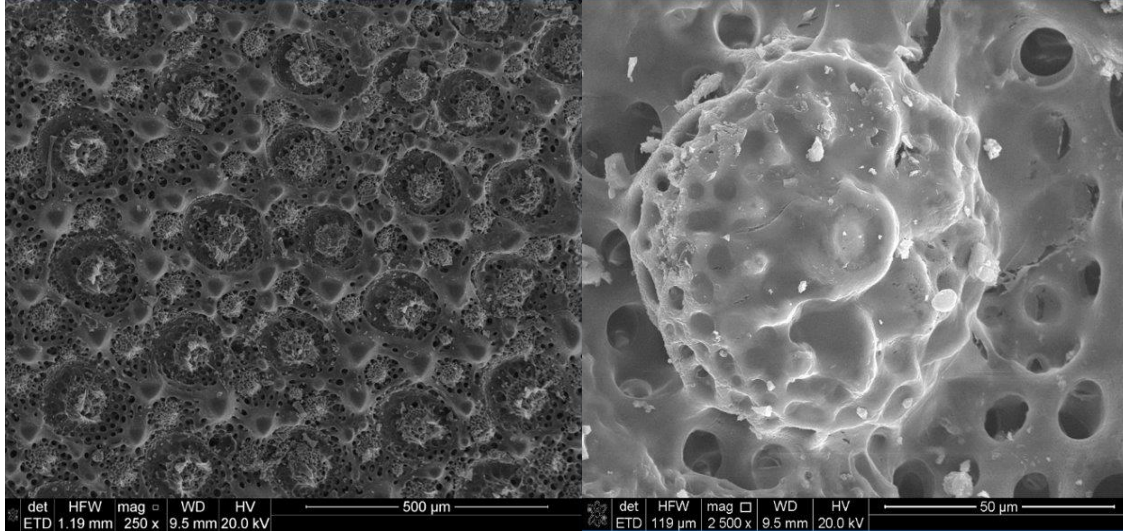


Figure 27. SEM pictures of the surface of Sand Dollar

Seashell has a large variety of types and Sand dollar is one of the most common type that can be found on the beach. Sand dollar refers to the type of urchins that are extremely flattened and can be commonly found on the beach. Their shell surfaces are usually bleached white by the sunlight after they become dead, the Sand Dollar is not necessarily white when they are alive and only the dead dry samples of the Sand Dollar were used in the experiment. SEM pictures shown in Figure 27 provide a brief look at the surface condition of sand dollar. The highly porous structure and the increased surface area can probably achieve high solar reflectance and enhance the heat dissipation. Similar to the desert snail, sand dollar is cover with Calcite (CaCO_3) plates. Therefore, under the situation of limit accessibility to desert snail shells, sand dollar is a well suit alternative. Since Calcite shows great reflectance in the solar spectrum of $0.28\mu\text{m}$ to $2.5\mu\text{m}$, where most of the solar irradiation energy is in, it can be an explanation to these creatures with shells to survive the brutal sun light. However, test results are still necessary to demonstrate the survivability comes from the shell reflectance to sunlight. Also, a question was brought up while in the test, which is how the thickness affects the shell reflectance. Then, due to the lack of thickness varieties, another alternative seashell was then analyzed. Marine Mollusk is one of the most common seashells and has large variety of shell thickness. We therefore used Marine Mollusks for the following study.

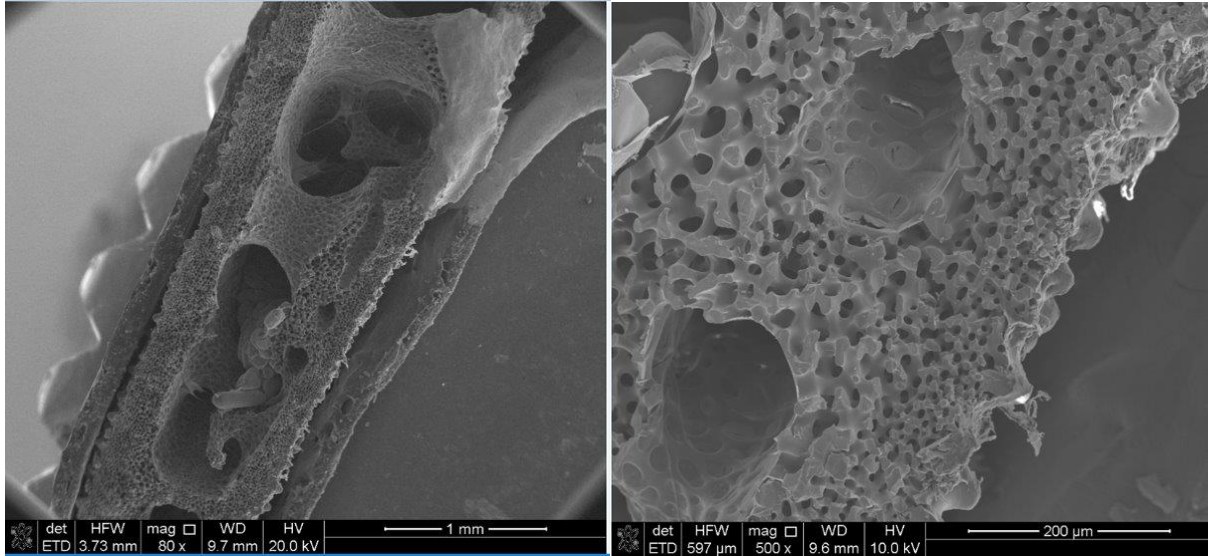


Figure 28. SEM pictures of Marine Mollusks cross section

Taking one step further, other factors that affect the shell reflectance are also analyzed with the purpose of gaining more benefits from learning the creatures with shells in nature. The SEM images above show the cross section of marine mollusks and highly porous structure is also observed in this case. A major percent of mollusks is known to live with shells and marine mollusks are quite accessible that various types of them can be found on the beach. As the mollusk shells are also composed of Calcite and with thickness of a wide range, they are also reasonable alternatives to the desert snails. Moreover, by comparing the measurement results of shells with different thickness, the shell thickness and even structural effects to the reflectance can be analyzed. Structural effect is significant when the two shells are comparable in the thickness, but it is also quite unlikely to be the only influence factor to the shell reflectance besides the shell thickness.

3.3 Spectrometer test result

After determining the sand dollar to be the target of the experiment at the beginning, the ability of passively cooling themselves from the direct sun light was analyzed by measuring the radiative properties of sand dollar in the spectrometer in the wavelength range of $0.25\mu\text{m}$ to $2.5\mu\text{m}$.

Since the purpose of this specific experiment is to analyze the shell radiative properties in the solar spectrum, therefore the minor changes of the shell surfaces should not affect the measurement

results. After measuring several samples with the spectrometer, a plot shows the typical radiative performance in the solar spectrum of sand dollar is created and shown below.

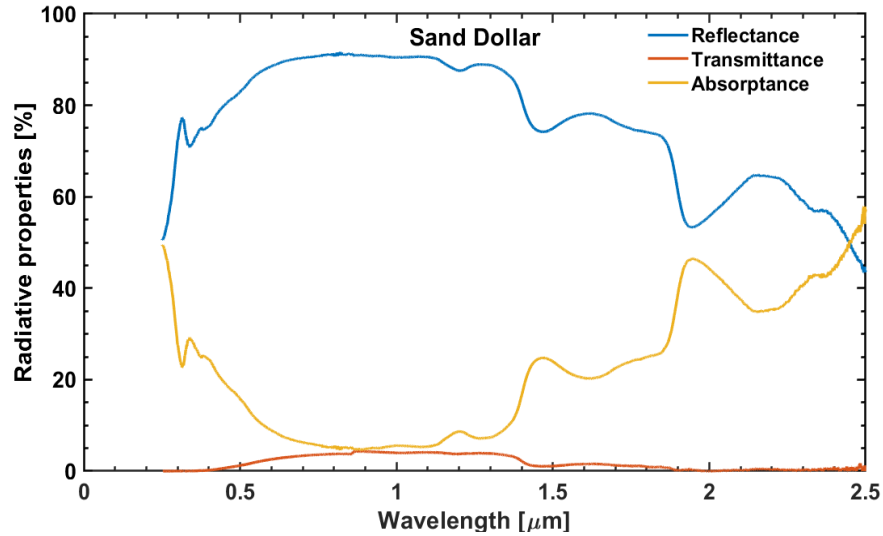


Figure 29. Radiative properties of sand dollar

As can be observed from the Figure 29, the reflectance is at more than 80% within the visible range from $0.38\mu\text{m}$ to $0.74\mu\text{m}$ and a part of NIR (Near infrared) range between $0.74\mu\text{m}$ and $1.4\mu\text{m}$. The peak reflectance reaches 91.7% at the wavelength around $0.82\mu\text{m}$. This result is not quite surprising to us considering about the high reflectance of Calcite materials. However, it is still worth digging deeper to find if there is any other factor affecting the reflectance of sand dollar in the solar spectrum. What is more, benefitting from the flattened surfaces of these pieces of Sand Dollar, the surface structure that may affect the measurement results could be assumed to be consistent amongst the sand dollar samples. Then since the sand dollar samples were all at similar thickness, where the thickness differences were too small to be detected by available tools like Vernier scale. Therefore, we were later obstructed by the limitation appeared in analyzing the possible thickness effect on the radiative properties of shells.

Departure from the Sand Dollar, a few of common types of shells were then used to continue the experiment. These shells are called white shell in the following paragraphs for the sake of distinguishing them from the sand dollar and also because of their white surfaces. At the same time, the color factor that may affect the measurement result is controlled as sand dollar is also

white as mentioned above. Covering a wide range of thickness, these shells from the dead marine mollusks are perfect targets to be used in the study of how the thickness affects shells radiative properties. The figure below shows the radiative properties of a thin white shell.

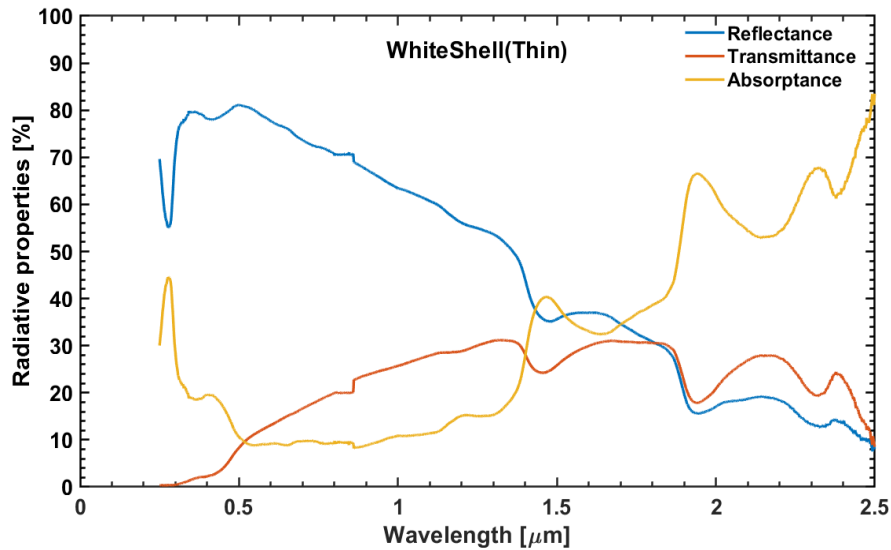


Figure 30. Thin white shell radiative properties

As shown in the Figure 30 the thin white shell has slightly less than 80% of reflectance in the visible range at the beginning, however the reflectance drops greatly after a short initial segment. This result shows that thin white shells are not ideal targets of studying the passive radiative cooling since their performance of the solar reflectance is far less than satisfying. The reason that they are able to survive from the sunlight can possibly be explained by the small surface area of their bodies, which is another type of protection to prevent them from receiving too much heat. Then, the thick white shells were measured in the spectrometer across the range of solar spectrum.

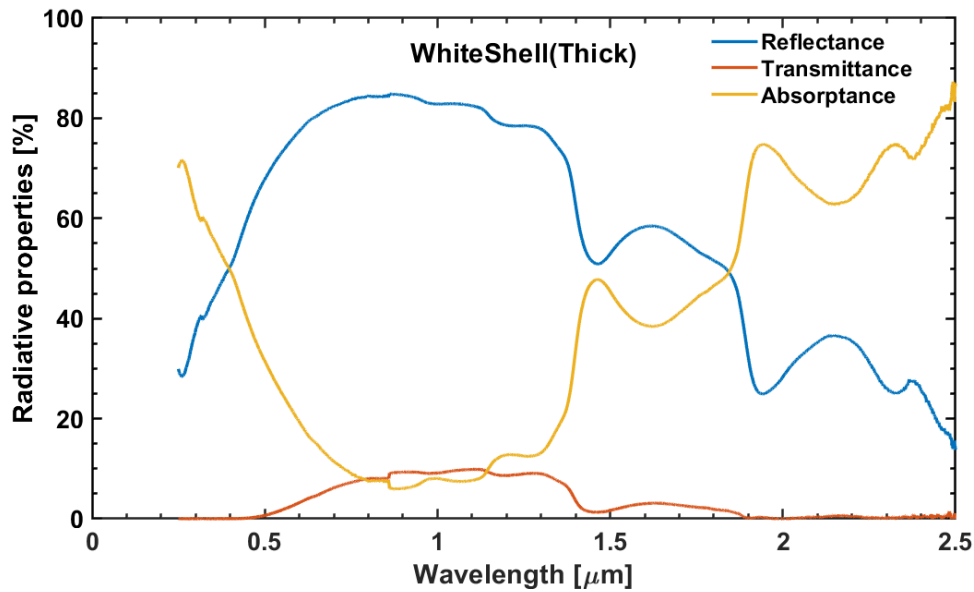


Figure 31. Thick white shell radiative properties

The measurement result of one of the thick white shell is shown in the Figure 31, which shows better reflectance performance in the solar spectrum than the thin white shells. The largest reflectance of thick shell is higher than the thin shell and the high reflectance covers a longer range of wavelength. Therefore, this result shows that the shell spectral response relies on the thickness and the improvement to the reflectance from the increase in thickness is significant.

Then the plot in Figure 32 shows the radiative properties of another thick white shell. The two thick shells are comparable in thickness and have similar overall reflectance trend in the solar spectrum. However, the radiative properties of two shells at the very beginning of the solar spectrum behave quite differently. A variant of possible factors can affect the radiative properties of shells while the thickness factor is controlled and the surface influence can be considered to be trivial because both of thick shells have white smooth surfaces. A very likely explanation to the difference can be the structural difference under the shells. To study the inside shell structural effect to the shell radiative properties is actually a long term project, so far the research on Bio-inspired passive cooling method has been focused on the Sand Dollar and white shell. In turn, it means that a larger species of creatures with shells need to be studied and most importantly how their shell inside structure determines their reflectance needs to be discovered. So that when there is a chance that a desert snail shell can be obtained and studied in the laboratory, some true

innovations in passive radiative cooling can be made from analyzing the desert snail shell matter composition and overall structure.

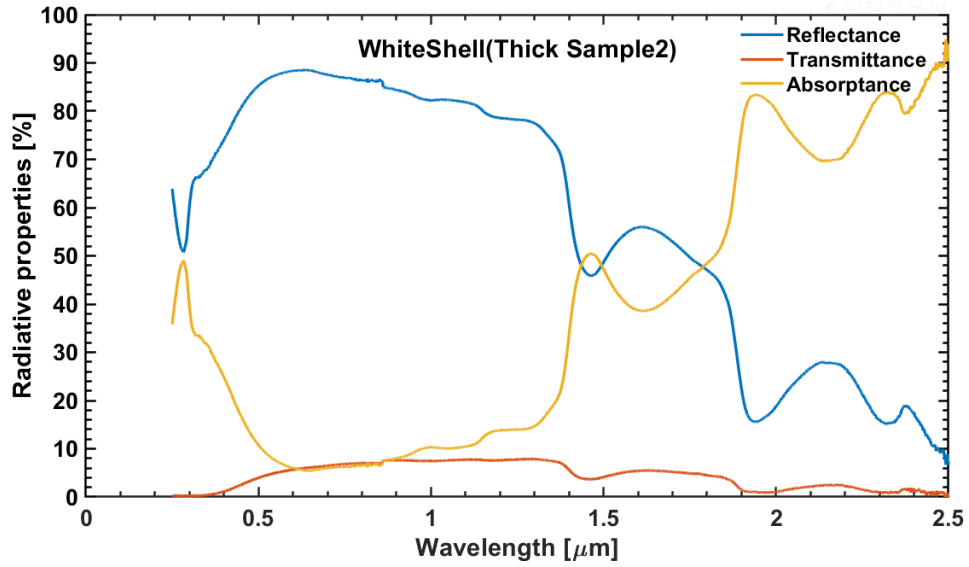


Figure 32. Second thick white shell sample radiative properties

4. CONCLUSION AND FUTURE WORK

In summary, partial daytime cooling in TiO₂ nanocomposite cooling paint is successfully demonstrated. Meanwhile, we recognize that a major problem for the TiO₂ paint absorption in the UV range. Then we develop BaSO₄-based colored cooling paints, by recognizing that BaSO₄ provides higher reflectance than TiO₂ that is commonly used in commercial paints. We have observed improvements in the radiative properties with our BaSO₄ nanocomposite paints compared to commercial color paints in spectrometry measurements. A theoretical prediction could be given that Light Green and Blue cooling paints should provide remarkably improved cooling effect compared to commercial Light Green and Blue paints. In the outdoor experiments, the reduced temperature of 4°C and 5°C below the commercial color paint temperature for Light Green and Blue cooling paint respectively was also observed, which is consistent with our results in spectrometry measurement results. Yellow and Green cooling paints also showed improved cooling effects, which were slightly less than Light Green and Blue cooling paints. Illustrated from both theoretical and experimental perspectives, our utilization of BaSO₄ nanoparticles as the basis of colored cooling paint has a confirmed contribution in achieving better cooling effect than commercial color paints. In the future, theoretical optimization of colored cooling paint utilizing the combination of MMT and MC will be considered as the major interest of research. The optimization is not just limited in achieving higher solar reflectance in the UV band, focus is also shared on optimizing the colored cooling paints from a broader scope including the particle density and particle size. Different optimization algorithms will be applied if necessary to ensure the reliability of optimized results.

At the same time, we will also pay attention to the access of real desert snail shells so that we can proceed to the next step in the study of Bio-inspired cooling method. So far, the experiment result shows that seashell thickness has a large impact on the shell radiative properties. Without knowing the exact influence of shell inner structure, more detailed conclusions cannot be made yet. In the next step, we will further study the structure effect on the shell cooling performance, it will be a great reference in our design of color paints. Moreover, since our Bio-inspired cooling method studies have been focused on shells, we expect to study the possible solutions from more different creatures. Butterfly can be a potential research of interest because of their high UV reflectance

wing [18]. Therefore, more insights from Bio-inspired cooling method will surely aid our work in manufacturing innovative radiative cooling paints.

APPENDIX A. SEM PICTURES

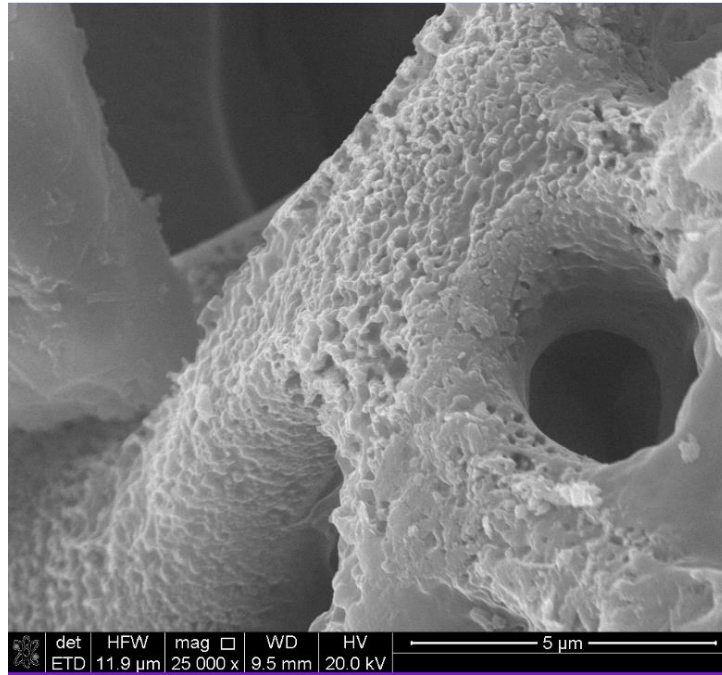


Figure 33. SEM picture of sand dollar with 25k Magnification

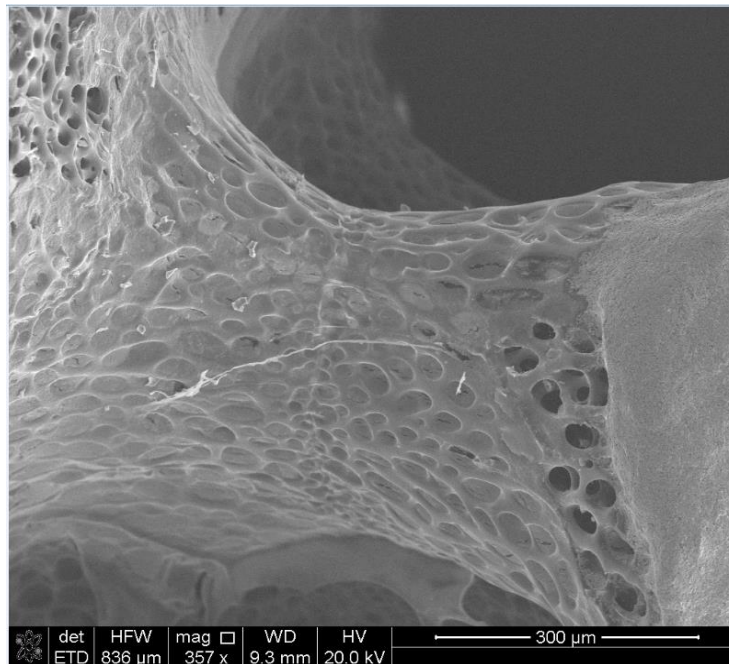


Figure 34. SEM picture of inside Marine mollusks with 357 Magnification

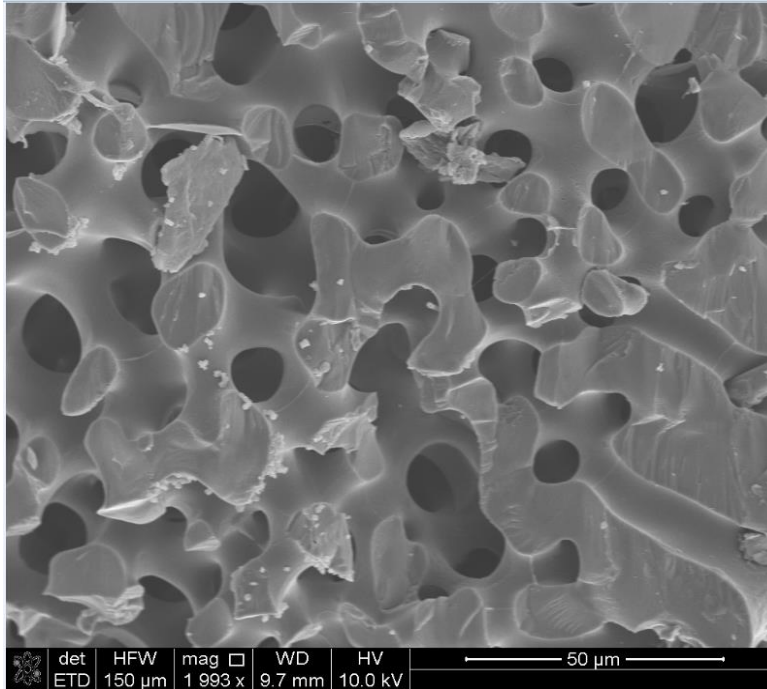


Figure 35. SEM picture of inside Marine Mollusks with 2K magnification

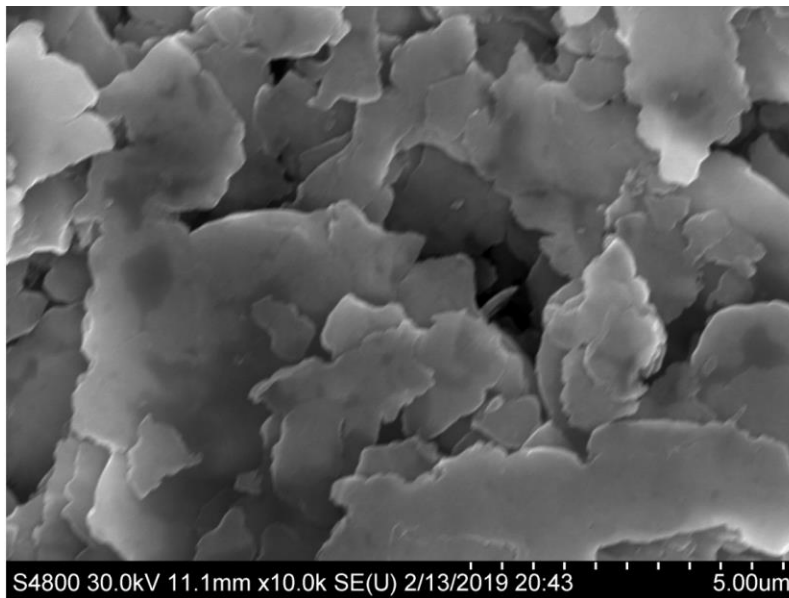


Figure 36. SEM picture of inside Marine Mollusks with 10K magnification

OPTIONAL SECTION

The appendix titles have a ‘Major Heading’ style applied. These will allow for an un-indented appearance in the table of contents. Tables and figures that appear within this section DO

NOT need to appear in the list of figures or tables. However, you may label your appendix figures/tables as Figure/Table A.1, Figure/Table A.2, etc. If you have multiple appendices please change the label letter with each new appendix (example: Figure A.1, Figure B.1, Figure C.1, etc.).

The Graduate School is fairly flexible with the appendix format. We just ask that text, figures, and tables fit within all margin requirements.

REFERENCES

- [1] J. Peoples, X. Li, X. Lv, J. Qiu, Z. Huang and X. Ruan, "A strategy of hierarchical particle sizes in nanoparticle composite for enhancing solar reflection," *International Journal of Heat and Mass Transfer*, vol. 131, pp. 487-494, 2019.
- [2] T. Nilsson, G. Niklasson and C. Granqvist, "A solar reflectin material for radiative cooling applications: ZnS pigmented polyethylene," *Solar Energy Materials and Soalr Cells*, vol. 28, no. 2, 1992.
- [3] A. P. Raman, M. Anoma, L. Zhu, E. Rephaeli and S. Fan, "Passive radiative cooling below ambient air temperature under direct sunlight," *Nature*, vol. 515, no. 7528, pp. 540-544, 2014.
- [4] Z. Huang and X. Ruan, "Nanoparticle embedded double-layer coating for daytime radiative cooling," *International Journal of Heat and Mass Transfer*, vol. 104, pp. 890-896, 2017.
- [5] J.-L. Kou, Z. Jurado, Z. Chen, S. Fan and A. J. Minnich, "Daytime Radiative Cooling Using Near-Black Infrared Emitters," *ACS Photonics*, vol. 4, no. 3, pp. 626-630, 2017.
- [6] Y. Zhai, Y. Ma, S. N. David, D. Zhao, R. Lou, G. Tan, R. Yang and X. Yin, "Scalable-manufactured randomized glass-polymer hybrid metamaterial for daytime radiative cooling," *Science*, vol. 355, no. 6329, pp. 1062-1066, 2017.
- [7] A. R. Gentle and G. B. Smith, "A Subambient Open Roof Surface under the Mid-Summer Sun," *Advanced Science*, vol. 2, no. 9, 2015.
- [8] J. Mandal, Y. Fu, A. C. Overvig, M. Jia, K. Sun, N. N. Shi, H. Zhou, X. Xiao, N. Yu and Y. Yang, "Hierarchically porous polymer coatings for highly efficient passive daytime radiative cooling," *Science*, vol. 362, no. 6412, pp. 315-319, 2018.
- [9] A. Leroy, B. Bhatia, C. C. Kelsall, A. Castillejo-Cuberos, M. D. C. H., L. Zhao, L. Zhang, A. M. Guzman and E. N. Wang, "High-performance subambient radiative cooling enabled by optically selective and thermally insulating polyethylene aerogel," *Science Advances*, 2019.
- [10] T. Li, Y. Zhai, S. He, W. Gan, Z. Wei, M. Heidarinejad, D. Dalgo, R. Mi, X. Zhao, J. Song, J. Dai, C. Chen, A. Aili, A. Vellore, A. Martini, R. Yang, J. Srebric, X. Yin and L. Hu, "A Radiative Cooling Structural Material," *Science (New York, N.Y.)*, vol. 364, no. 6442, pp. 760-763, 2019.
- [11] B. Bhatia, A. Leroy, Y. Shen, L. Zhao, M. Gianello, D. Li, T. Gu, J. Hu, M. Soljačić and E. N. Wang, "Passive directional sub-ambient daytime radiative cooling," *Nature Communications*, vol. 9, no. 1, 2018.
- [12] T. Ung, L. M. Liz-Marzan and P. Mulvaney, "Gold nanoparticle thin films," *Colloids and Surfaces A: Physicochemical and Engineering Aspects*, 2001.
- [13] A. Harrison and M. Walton, "Radiative cooling of TiO₂ white paint," *Solar Energy*, vol. 20, no. 2, pp. 185-188, 1978.
- [14] R. D. Jackson, T. R. Clarke and M. S. Moran, "Bidirectional calibration results for 11 spectralon and 16 BaSO₄ reference reflectance panels," *Remote Sensing of Environment*, vol. 40, no. 3, pp. 231-239, 1992.

- [15] N. N. Shi, C.-C. Tsai, F. Camino, G. D. Bernard, N. Yu and R. Wehner, "Keeping cool: Enhanced optical reflection and radiative heat dissipation in Saharan silver ants," *Science*, vol. 349, no. 6245, pp. 298-301, 2015.
- [16] L. Wang, S. L. Jacques and L. Zheng, "MCML—Monte Carlo modeling of light transport in multi-layered tissues," *Computer Methods and Programs in Biomedicine*, vol. 47, no. 2, pp. 131-146, 1995.
- [17] M. R. Islam, S.-N. K., A. Team, S. M. V. d. Walt, S. Singh, Sherry and M. Salah, "Shell protects from heat : Snails And Slugs," *AskNature*, 2007.
- [18] H. Ghiradella, D. Aneshansley, T. Eisner, R. Silberglied and H. E. Hinton, "Ultraviolet Reflection of a Male Butterfly: Interference Color Caused by Thin-Layer Elaboration of Wing Scales," *Science*, vol. 179, no. 4071, p. 415, 1973.